

Radiatively driven relativistic jets with variable adiabatic index equation of state

Mukesh K. Vyas¹, Rajiv Kumar¹, Samir Mandal², Indranil Chattopadhyay¹

¹*Aryabhatta Research Institute of Observational Sciences (ARIES), Manora Peak, Nainital-263002, India*

²*Indian Institute of Space Science & Technology (IIST), Trivandrum, India.*

ABSTRACT

We investigate a relativistic fluid jet driven by radiation from a shocked accretion disc around a non-rotating black hole approximated by Paczyński-Wiita potential. The sub-Keplerian and Keplerian accretion rates control the shock location and therefore, the radiation field around the accretion disc. We compute the radiative moments with full special relativistic transformation. The effect of a fraction of radiation absorbed by the black hole has been approximated, over and above the special relativistic transformations. We show that the radiative moments around a super massive black hole are different compared to that around a stellar mass black hole. We show that the terminal speed of jets increases with the mass accretion rates, synchrotron emission of the accretion disc and reduction of proton fraction of the flow composition. To obtain relativistic terminal velocities of jets, both thermal and radiative driving are important. We show for very high accretion rates and pair dominated flow, jets around super massive black holes are truly ultra-relativistic, while for jets around stellar mass black holes, terminal Lorentz factor of about 10 is achievable.

Key words: Black Holes, Jets and outflows, Hydrodynamics, Radiation dynamics, Shock waves

1 INTRODUCTION

Astrophysical jets are ubiquitous, as they are associated with many classes of astrophysical objects such as active galactic nuclei (AGN e.g., M87), young stellar objects (YSO e.g., HH 30, HH 34), X-ray binaries (e.g., SS433, Cyg X-3, GRS 1915+105, GRO 1655-40) etc.

However, only jets around X-ray binaries like GRS1915+105 (Mirabel & Rodriguez 1994) and AGN like 3C273, 3C345 (Zensus *et al.* 1995), M87 (Biretta 1993) etc are relativistic. In this paper we concentrate on relativistic jets. Since it is conjectured that stellar mass black hole reside at the heart of microquasars and those of the super-massive variety dictates the dynamics of the AGNs/quasars, therefore it implies that a jet has to originate from the accreting matter itself, since black holes (hereafter, BH) have neither hard surface nor any atmosphere. Interestingly, simultaneous radio and X-ray observations of microquasars show a very strong correlation between the spectral states of the accretion disc and the associated jet states (Gallo *et. al.* 2003; Fender *et al.* 2010; Rushton *et al.* 2010), which reaffirms the fact that jets do originate from the accretion disc. In addition, recent observations have shown that jets originate from a region which is less than 100 Schwarzschild radii (r_g) around the unresolved central object (Junor *et. al.* 1999; Doeleman *et. al.* 2012), which imply that the entire disc may not participate in production of jets, but only the central region of the disc is responsible.

Since jets are supposed to originate very close to the central object, the plasma at the base should be hot and is expected to be fully ionized. This hot outflowing plasma will also be in the intense radiation field from the accretion disc. A number of scientists have studied the interaction of radiation with jets. Icke (1980) ignored radiation drag and investigated particle and gas flow in the radiation field of an underlying Keplerian disc (Shakura & Sunyaev 1973). Sikora & Wilson (1981) studied the interaction of the particle jets with the radiation field, in the funnel like region of a thick accretion disc (Paczynski & Wiita 1980). Ignoring gravity and for normal electron-proton or $e^- - p^+$ plasma jets, the authors achieved a terminal speed of around $v_T \sim 0.4c$, and obtained terminal Lorentz factor $\gamma_T \sim 3$ for electron-positron or, $e^- - e^+$ plasma. In a seminal paper, Icke (1989) showed that for particle jets above an infinite Keplerian disc, the radiation drag ensures an upper limit of terminal speed, which the author termed it as ‘magic speed’ and which turned out to be $v_{\text{magic}} = 0.45c$. The much ‘vaunted’ magic speed is actually the so-called equilibrium speed of jet plowing through a radiation field near the Keplerian disc surface. It may be noted that, equilibrium speed (v_{eq}) is the speed of the jet at which the radiation force becomes zero and for speeds above which, radiative deceleration sets in. Equilibrium speed arises due to the presence of the radiation drag. Radiation drag is significant for a radiation field due to an extended source. On the other hand, terminal speed (v_T) is the speed of the jet at which the total force on the jet approaches zero. Therefore, the jet may achieve v_T only at large distances away from

the central object, while it may reach v_{eq} at distances much closer to the central object. Melia & Königl (1989) considered jets which are accelerated to ultra-relativistic speed way above the local v_{eq} . This causes the radiation drag to become effective and decelerate the jet to terminal velocity $v_T \sim 0.995$. Sikora *et al.* (1996) concluded that for the disc they chose, the maximum possible of Lorentz factor is ≤ 4 . The Japanese group led by Jun Fukue made very important contribution to the research of transonic outflows, both in the relativistic, as well as, in non-relativistic domain. Fukue (1996) extended Icke's work, and studied particle jets away from the axis, although like Icke, considered near disc approximation for the radiation field above it. The actual terminal jet velocity achieved was $v_T \lesssim v_{\text{magic}}$, which is expected. However, the main problem is the tendency of the radiation field to spin up the jet and thereby spreading the jet. Fukue (1999) then studied jets confined by disc corona in order to arrest the spreading and collimate the jet. Hirai & Fukue (2001) on the other hand, computed the radiation field due to a Keplerian disc governed by Newtonian gravity, Schwarzschild gravity and Kerr gravity. The strength of the radiation field above the disc, described by Schwarzschild gravity is 50% lesser than that due to Newtonian gravity. But the strength of the radiation field above a disc governed by a Kerr type gravity is 10 times higher than that due to the Newtonian gravity, making radiatively driven jets easier to blow for a rotating black hole. In a very interesting paper, Fukue *et al.* (2001) considered a hybrid disc, consisting of outer Keplerian disc and inner advection dominated accretion flow or ADAF (Narayan *et al.* 1997) type accretion solutions. Since ADAF is dimmer, so the inner region from which the electron-positron jet is assumed to emerge in this paper, does not contribute in the radiation field. Such a scenario do produce jets with terminal Lorentz factor $\gamma_T \sim 2$, and the radiation field from the outer Keplerian disc also helps in collimation.

Along with the various disc models like Keplerian disc, thick disc, ADAF, investigations on advective discs was initiated by Liang & Thompson (1980); Fukue (1987); Chakrabarti (1989). Such a disc can admit smooth solutions, and for the right choice of parameters it may harbour shock transition. This disc model was extended by considering injection of a mixture of matter with Keplerian angular momentum and sub-Keplerian angular momentum. The portion of disc which is termed as sub-Keplerian disc (SKD), sandwiches the Keplerian disc (KD) from the top and the bottom (see Fig. 1). SKD may undergo shock transition and at the shock, KD terminates due to extra heating in the post-shock disc or PSD (Chakrabarti & Titarchuk 1995). Although it was initially proposed as an elaborate and contrived model solution, but was recently confirmed by numerical simulation

(Giri & Chakrabarti 2013). Interaction of radiations with the outflowing jet from PSD was studied by Chattopadhyay & Chakrabarti (2000a,b, 2002). The investigation of outflowing jet (Chattopadhyay *et al.* 2004; Chattopadhyay 2005) was further elaborated for the radiation field of the Chakrabarti-Titarchuk type hybrid disc (Chakrabarti & Titarchuk 1995). Generally most of the papers which investigate the interaction of jet with disc photons do not consider the issue of the launch mechanism of jets in terms of the accretion properties. In the advective disc regime, numerical simulations first showed that the extra-thermal gradient force in the PSD automatically generates bipolar outflows (Molteni *et al.* 1994, 1996; Das *et al.* 2014). Theoretically too, for a viscous advective disc, the mass outflow rate of bipolar outflow was computed in terms of various accretion disc parameters (Chattopadhyay & Das 2007; Kumar & Chattopadhyay 2013; Kumar *et al.* 2013). However, jets emerging from the PSD in the steady state and hydrodynamic limit are weak. On the other hand, if the emanating jets are simultaneously acted on by disc photons, then the jets obtained are stronger (Kumar *et al.* 2014). In fact, it has been shown by Kumar *et al.* (2014), that as the advective disc spectral state moves from low-hard or LH state to intermediate states or IM, the steady jet becomes stronger, as has been reported in observations (Gallo *et al.* 2003; Fender *et al.* 2010; Rushton *et al.* 2010). In other words, Kumar *et al.* (2014) not only generated jets from accretion solutions, but also accelerated the jets by depositing momentum of disc photons on to the jet. However, the formalism followed by Kumar *et al.* (2014) is only correct up to the first order of v/c , where v is the flow velocity. So solving the jet equations in the relativistic hydrodynamic limit is warranted for Chakrabarti-Titarchuk type disc.

The equations of motion of radiation hydrodynamics were developed by many authors (Hsieh & Spiegel 1976; Mihalas & Mihalas 1984; Kato *et al.* 1998). It was observed that in the non-relativistic limit, only flux of the radiation pushes matter. In the relativistic limit and optically thin plasma, the moving plasma is pushed by the flux and is dragged by the energy density and pressure of the radiation field. The radiation transfers momentum on to the electrons and therefore, the radiative acceleration term is proportional to the number density of electrons/positrons in the jet, which is true in relativistic, as well as, non-relativistic limit. But in relativistic limit, the radiative acceleration term is also proportional to the inverse of the enthalpy of the flow, which marks a major difference between relativistic and non-relativistic domain. Therefore, although Kumar *et al.* (2014) showed radiatively driven jets qualitatively explain the correlation between jet states and the spectral state of the ac-

cretion discs, but a correct relativistic narrative is required. If however, one considers the gas pressure (p) to be negligible compared to the radiation pressure (P^{ij}), then even in the fully relativistic limit, the net radiative term is only proportional to the number density of the flow. Therefore, the physics of interaction of disc radiation with a fluid jet in the relativistic regime is qualitatively and quantitatively different than that between radiation and jet in the non-relativistic domain (Chattopadhyay & Chakrabarti 2002; Kumar *et al.* 2014), or relativistic jets in the domain where $P_{ij} \gg p\delta_{ij}$ (Chattopadhyay *et al.* 2004; Chattopadhyay 2005). In this paper, we would like to investigate this phenomenon in details. Ferrari *et al.* (1985) studied interaction of fluid jets with the disc radiation but the jet fluid was described by fixed adiabatic index Γ and Newtonian gravitational potential. However, fixed Γ is an artifact of non-relativistic kinetic theory, *i.e.*, if the internal random motions of the particles in the fluid is relativistic, then Γ is a function of temperature (Chandrasekhar 1938; Synge 1957), where, for relativistic temperatures, the flow is described by $\Gamma \sim 4/3$ and for non-relativistic temperatures $\Gamma = 5/3$. Taub (1948) showed that it is unphysical to consider a fixed Γ to describe fluid with several orders of magnitude variation in temperature. Moreover, it has also been shown that, not only temperature, relativistic nature of the thermal energy depends also on the composition of the flow (Chattopadhyay 2008; Chattopadhyay & Ryu 2009; Chattopadhyay & Chakrabarti 2011; Kumar *et al.* 2013; Chattopadhyay *et al.* 2013; Kumar & Chattopadhyay 2014). Infact it was shown that, contrary to expectation, pair-plasma is thermally the least relativistic, and to make a flow more relativistic one needs baryons in addition to electrons or positrons, and the fluid with proton number density around 27% of that of electrons is thermally the most relativistic. Now radiation force is imparted mainly onto the electrons and positrons which should make the lighter jet to move faster due to inertia, as is shown for cold jets (Chattopadhyay *et al.* 2004; Chattopadhyay 2005). On the contrary, the thermodynamics of the jet will make the fluid with 27% proton content to be more relativistic. So in presence of radiation driving, would a jet with protons less than 27% be more accelerated, or, the thermal nature of the flow dictate the dynamics. Additionally for fluid jets, the pressure gradient force should accelerate the jet, while gravity decelerate, and radiative force depends on the fluid speed in addition to the radiative moments. At the base, the jet is supposed to be hot, so initially, can the jet be thermally driven to speeds above v_{eq} , and therefore, is mostly decelerated by radiation and not accelerated at all? In short, can disc radiation power jets to relativistic terminal speeds? These are few of the various issues we would like to investigate in this paper. In this paper

the accretion disc plays an auxiliary role, *i.e.*, we do not employ a self consistent calculation of accretion-ejection system, rather the jet is assumed to originate in the inner disc, which in our case is PSD, and the accretion disc just provides the radiation field which interacts with the jet. While doing so, we have not increased the number of accretion disc parameters, and the shock location is estimated from the SKD accretion rate, and PSD luminosity has been estimated from the accretion rates from SKD and KD.

In the next section, we present the simplifying assumptions and various equations. In section 2.1, we present the governing equations of the jet. In section 2.2, we present the model of accretion disc, estimation of the disc intensity from various disc components (section 2.2.1), and computation of the radiative moments (section 2.2.2) from the disc intensities. Disc intensities, the disc velocity and temperature profiles are estimated in Appendix A. The post-shock intensity is estimated in Appendix B. In section 3, we present the solution methodology and in section 4, we present the results and in the last section (5) we discuss the physical implications of the obtained results and draw concluding remarks.

2 ASSUMPTIONS, GOVERNING EQUATIONS OF JET & STRUCTURE OF ACCRETION DISC

The space time metric is given by

$$ds^2 = -c^2 dt^2 + dr^2 + r^2 d\phi^2 + dz^2 \quad (1)$$

where, t , r , ϕ , z are the time, radial, azimuthal and the axial coordinates. The jet is considered to be in steady state (*i.e.*, $\partial/\partial t = 0$). The above is a special relativistic metric. Although the jets originate close to the central compact object, but it traverses to distances where the effect of gravity is negligible. Hence pseudo potential is used to take care of gravity in the equations of motion, such that at close ranges the gravity limits the outward thrust, and at large distances it is just special relativistic regime, therefore one may avoid general relativistic complications and still be accurate enough. Moreover, the jets are collimated, so we consider on-axis (*i.e.*, $u^r = u^\phi = \partial/\partial r = 0$) and axis-symmetric ($\partial/\partial \phi = 0$) jet. Without any loss of generality, the jet is assumed to expand radially along the z -axis, the value of any jet variable on any particular point of the axis, is assumed to be maintained along its breadth at the same z . In the present effort, we just assume that there are jets from an accretion disc, but do not compute jets self consistently from accretion solution. The accretion disc is present but plays a supportive role, by supplying the radiation which

[h]

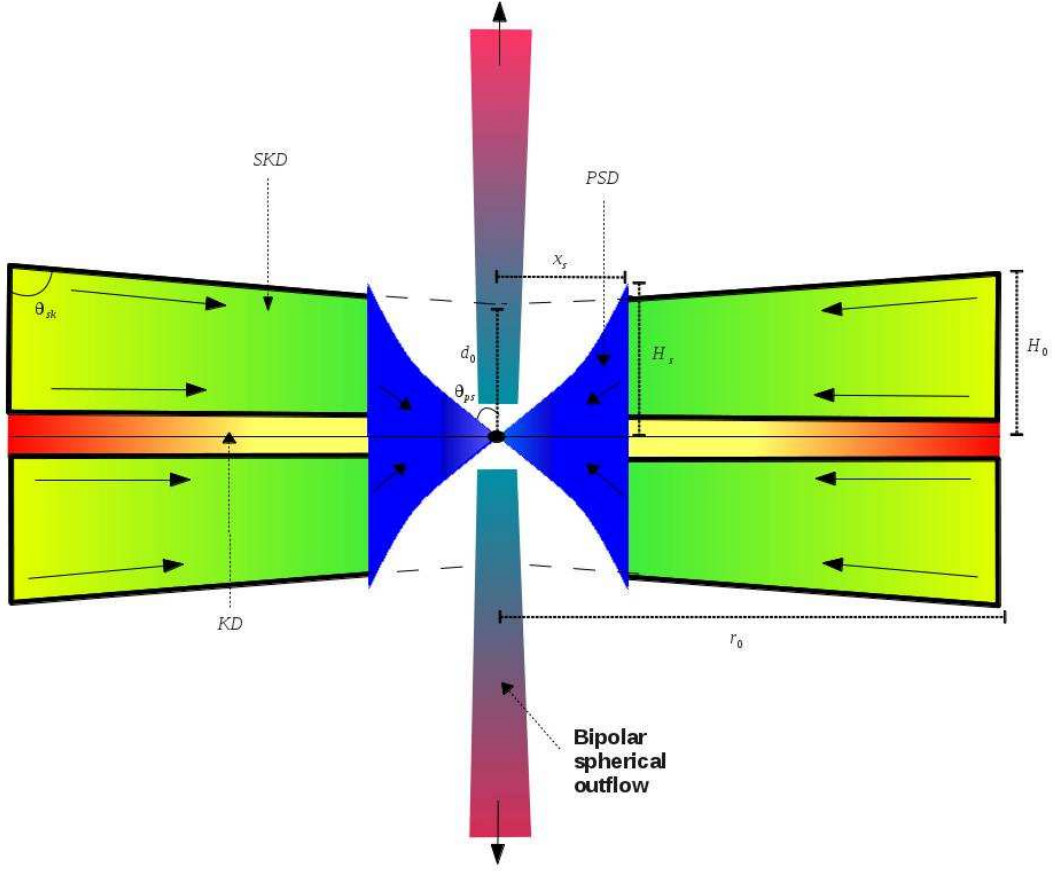


Figure 1. Cartoon diagram of cross-sections of axis-symmetric accretion disc and the associated jet in (r, ϕ, z) coordinates. The Keplerian disc (KD), sub-Keplerian disc (SKD), and the post-shock disc (PSD) are broadly the three regions of the disc. The shock location x_s , the intercept of SKD on the axis (d_0), height of the shock H_s are shown, the outer edge of the disc r_0 are all marked. Semi-vertical angle of PSD is θ_{ps} and for SKD it is θ_{sk} . The gradient of colour represents low temperature (red) to high temperature (blue).

drives the jet. In the next subsection we present the equations of motion. We present the description of the accretion disc and the method to compute radiative moments at section 2.2.

2.1 Equations of motion of the jet

The energy momentum tensor of the jet and the radiation field is given by

$$T_M^{\alpha\beta} = (e + p)u^\alpha u^\beta + pg^{\alpha\beta}; \quad T_R^{\alpha\beta} = \int I_\nu l^\alpha l^\beta d\nu d\Omega, \quad (2)$$

where, suffix M stands for jet material and R stands for radiation field. The internal energy of the jet is e and p is the isotropic pressure of the jet fluid, the metric tensor components are given by $g^{\alpha\beta}$ and u^α is the four velocity. Furthermore, I_ν is the specific intensity of the radiation field, l^α s are the directional derivatives, ν the frequency of the radiation and Ω is

the solid angle subtended by the field point on to the source point. By definition, field point is where the moments are computed, while source point is the location of the source of the radiation. The equations of motion are given by

$$T_{;\beta}^{\alpha\beta} = 0 = (T_R^{\alpha\beta} + T_M^{\alpha\beta})_{;\beta} \quad (3)$$

From the above equation, the momentum conservation equation, in the i^{th} direction is obtained by using projection tensor $(g_\alpha^i + u^i u_\alpha)$, *i.e.*,

$$(g_\alpha^i + u^i u_\alpha) T_{M;\beta}^{\alpha\beta} = -(g_\alpha^i + u^i u_\alpha) T_{R;\beta}^{\alpha\beta} \quad (4)$$

Similarly, the energy conservation equation is obtained by taking

$$u_\alpha T_{M;\beta}^{\alpha\beta} = -u_\alpha T_{R;\beta}^{\alpha\beta} \quad (5)$$

The derivation of the equations of motion of radiation hydrodynamics for optically thin plasma, using above preliminaries, was investigated by a number of workers. Since we study on axis jet, the equations of motion greatly simplifies. The momentum balance equation (equation 4), in steady state and for on axis jet becomes;

$$(e + p) \left(u^z \frac{du^z}{dz} + \frac{GM_B}{(z - r_g)^2} \right) = -\frac{dp}{dz} - u^z u^z \frac{dp}{dz} + \rho_e \frac{\sigma_T}{m_e c} \mathfrak{S}^z. \quad (6)$$

The term containing M_B in the r. h. s of equation (6) is the Paczyński-Wiita term mimicking the gravity of non-rotating BH (Paczyński & Wiita 1980). The energy conservation equation (5) in the scattering regime is,

$$\frac{de}{dz} - \frac{e + p}{\rho} \frac{d\rho}{dz} = 0 \quad (7)$$

where, ρ is the total mass density, ρ_e is the leptonic mass density of the flow and m_e is the electron rest mass. Similarly, from continuity equation the mass outflow rate is given as

$$\dot{M}_{out} = \rho u^z \mathcal{A}, \quad \mathcal{A} \propto z^2 \text{ for radial, narrow jet about the axis!} \quad (8)$$

In above equations, G , M_B , σ_T , $r_g = 2GM_B/c^2$ and \mathcal{A} are the universal gravitational constant, the mass of the central black hole, Thomson scattering cross-section, Schwarzschild radius and cross section of the jet respectively. \mathfrak{S}^z is the net radiative contribution and is given by;

$$\begin{aligned} \frac{\sigma_T}{m} \frac{\mathfrak{S}^z}{c} &= \frac{\sigma_T}{m_e} \left[\gamma \frac{F^z}{c} - \gamma^2 u^z E - u_j P^{zj} + u^z \left(2 \frac{\gamma}{c} u_j F^j - u_j u_k P^{jk} \right) \right] \\ &= [\gamma(1 + 2u^z u_z) \mathcal{F} - \gamma^2 u^z \mathcal{E} - \mathcal{P}(u_z + u^z u_z u_z)] \text{ for on axis jet!} \end{aligned} \quad (9)$$

In above equations, E , F^z , and P^{zz} are the radiative energy density, the radiative flux and the radiative pressure tensor measured in observer frame, and $\mathcal{E} = \frac{\sigma_T}{m_e} E$, $\mathcal{F} = \frac{\sigma_T}{m_e c} F^z$, and $\mathcal{P} = \frac{\sigma_T}{m_e} P^{zz}$. Furthermore, γ ($\equiv -u_t = \sqrt{1 + u_i u^i}$) is the Lorentz factor.

It may be noted that, we have assumed the jet to be flowing radially out within a conical surface for simplicity, since our primary concern is to investigate the respective role played by thermal and radiative driving terms on jet dynamics. Needless to say depending upon initial condition and disc radiation field, the jet geometry may depart from the simple geometry we are following in this paper. Even then, our assumption is not completely outlandish. The funnel like surface of the PSD is the region from where the jet is supposed to originate, the shape itself will arrest the lateral spread of the outflowing matter. Moreover, such shape causes the r component of radiative flux directed towards the axis (Chattopadhyay 2005) which would also reduce the lateral spreading even with high jet-base temperature. However, one can justify our assumption only if we solve the jet equations since we need some estimate of the pressure. In appendix (D), we estimated the pressure gradient term along with the radiative term along r and compared them, the assumption of conical jet cross-section seems to hold.

2.1.1 Equation of state and the final form of equations of motion

The physics of the jet propagating in the radiation field of the accretion disc can be understood, if equations (6-8) are simultaneously solved. However, one has also to supply a closure relation *i.e.*, a relation between e , p , ρ called the equation of state (EoS) in order to solve equations (6-8). An EoS for multispecies, relativistic flow proposed by Chattopadhyay (2008); Chattopadhyay & Ryu (2009) is adopted, and is given by,

$$e = n_{e-} m_e c^2 f \quad (10)$$

with n_{e-} is the electron density and f is given by

$$f = (2 - \xi) \left[1 + \Theta \left(\frac{9\Theta + 3}{3\Theta + 2} \right) \right] + \xi \left[\frac{1}{\eta} + \Theta \left(\frac{9\Theta + 3/\eta}{3\Theta + 2/\eta} \right) \right] \quad (11)$$

Here, non-dimensional temperature is defined as $\Theta = kT/(m_e c^2)$, k is the Boltzmann constant and $\xi = n_{p+}/n_{e-}$ is the relative proportion of protons with respect to the number density of electrons. The mass ratio of electron and proton is $\eta = m_e/m_{p+}$. It is easy to see that by putting $\xi = 0$, we generate EoS for relativistic $e^- - e^+$ plasma (Ryu *et al.* 2006).

The expressions of the polytropic index N , adiabatic index Γ and adiabatic sound speed a are given by

$$N = \frac{1}{2} \frac{df}{d\Theta}; \quad \Gamma = 1 + \frac{1}{N}; \quad \frac{a^2}{c^2} = \frac{\Gamma p}{e + p} = \frac{2\Gamma\Theta}{f + 2\Theta}. \quad (12)$$

This EoS is an approximated one, and the comparison with the exact one shows that this EoS is very accurate (appendix C). Additionally, being algebraic and avoiding the presence of complicated special functions, this EoS is very easy to be implemented in simulation codes, as well as, be used in analytical investigations (Chattopadhyay & Ryu 2009; Chattopadhyay & Chakrabarti 2011; Ryu *et al.* 2006; Chattopadhyay *et al.* 2013). The jet plasma is fully ionized. Therefore the interaction with photons would be dominated by scattering. Therefore, the energy equation (7) has no source term because in the scattering regime and in absence of emission/absorption, the r. h. s is zero and the flow is isentropic (Mihalas & Mihalas 1984). Under such conditions, equation (7) along with equation (10) can be integrated to obtain the relativistic isentropic equation of state,

$$\rho = \mathcal{C} \exp(k_3) \Theta^{3/2} (3\Theta + 2)^{k_1} (3\Theta + 2/\eta)^{k_2},$$

where, $k_1 = 3(2 - \xi)/4$, $k_2 = 3\xi/4$, $k_3 = (f - \tau)/(2\Theta)$, $\tau = (2 - \xi + \xi/\eta)$ and \mathcal{C} is the constant of entropy. We replace ρ from the above equation on to equation (8), we get the expression for entropy-accretion rate,

$$\dot{\mathcal{M}}_{out} = \frac{\dot{M}_{out}}{\text{geom.const.}\mathcal{C}} = \exp(k_3) \Theta^{3/2} (3\Theta + 2)^{k_1} (3\Theta + 2/\eta)^{k_2} u^z z^2 \quad (13)$$

This is also a measure of entropy of the jet and remains constant along the jet. We adopt a unit system where, the unit of speed is c , unit of length $r_g = 2GM_B/c^2$ and the unit of mass is M_B . Henceforth we write all equations in this unit system, except where it is explicitly mentioned. The three-velocity v is given by $v^2 = -u_i u^i / u_t u^t = -u_z u^z / u_t u^t$, *i.e.*, $u^z = u_z = \gamma v$. Now using energy conservation equation (7) along with the equation of state (10), the gradient of temperature of jet is given by,

$$\frac{d\Theta}{dz} = -\frac{\Theta}{N} \left[\frac{\gamma^2}{v} \left(\frac{dv}{dz} \right) + \frac{2}{z} \right] \quad (14)$$

The momentum balance equation (6), with the help of equations (10), (12) and (14), becomes

$$\begin{aligned} \gamma^4 v \left(1 - \frac{a^2}{v^2} \right) \frac{dv}{dz} &= \frac{2\gamma^2 a^2}{z} - \frac{1}{2(z-1)^2} \\ &+ \frac{\gamma^3 (2 - \xi)}{f + 2\Theta} [(1 + v^2)\mathcal{F} - v(\mathcal{E} + \mathcal{P})] \\ &= a_t + a_g + a_r. \end{aligned} \quad (15)$$

The l. h. s is the net acceleration term of a steady state jet. On the r. h. s, the first term is the thermal term $a_t = 2\gamma^2 a^2/z$ and it accelerates, while the second being gravity $a_g = -0.5/(z-1)^2$, it decelerates. The third term in r.h. s is the radiative term $a_r = \gamma^3 \tau [(1+v^2)\mathcal{F} - v(\mathcal{E} + \mathcal{P})]/(f+2\Theta)$. The radiative contribution is within the square bracket and the rest represents the interaction of matter jet with the radiation field. The physical significance of the term in the square bracket term is worth noticing. It has the form

$$(1+v^2)\mathcal{F} - v(\mathcal{E} + \mathcal{P})$$

The term proportional to v comes with a negative sign and would decelerate and is called the radiation drag term. If the first term $(1+v^2)\mathcal{F}$ dominates, then radiation would accelerate the flow, which means the net radiative term would either be accelerating or decelerating depending on the velocity. The dependence of radiative term on v arises purely due to relativity. In the purely non-relativistic domain *i.e.*, $v \ll 1$, the radiative term is just \mathcal{F} . In the fast but sub relativistic domain *i.e.*, $v^2 \ll 1$ the radiative term is $\mathcal{F} - v(\mathcal{E} + \mathcal{P})$ similar to the formalism followed by Chattopadhyay & Chakrabarti (2002); Kumar *et al.* (2014). The drag term arises due to the resistance faced by the moving material through the radiation field, and the finite value of the speed of light. Much talked about equilibrium speed v_{eq} is when $a_r = 0$, *i.e.*,

$$v_{eq} = \Re - \sqrt{\Re - 1}; \text{ where, } \Re = \frac{\mathcal{E} + \mathcal{P}}{2\mathcal{F}}. \quad (16)$$

From equation (16), it is clear that if the relative contribution of radiative moments or \Re approaches 1, *i.e.*, $\mathcal{F} = \mathcal{E} = \mathcal{P}$, then $v_{eq} \rightarrow 1$, *i.e.*, no radiation drag. Therefore, the nature of the quantity \Re dictates, whether a radiation field would accelerate a flow or decelerate it. Of course the resultant acceleration depends on the magnitude of all moments. There is an added feature of radiatively driven relativistic fluid, *i.e.*, the radiative term is multiplied by a term inverse of enthalpy ($\{f+2\Theta\}/\tau$) of the flow, which actually suggests that the effect of radiation on the jet is less for hotter flow.

2.2 Accretion disc and radiative moments

The accretion disc model considered here is the hybrid disc of the Chakrabarti-Titarchuk flavour (Chakrabarti & Titarchuk 1995; Giri & Chakrabarti 2013). In Fig. 1, we show all the components of the disc, *i.e.*, PSD, SKD and KD. The SKD flanks the KD, but mingles and forms the single component PSD. The colour coding represents lower (red) to higher (blue) temperature. The outer edge of the disc is r_0 where the disc height is H_0 . The inner

edge of SKD and KD is the shock location x_s , the inner edge of PSD say r_{in} is in principle the horizon, but we have considered it to be $r_{\text{in}} = 1.5r_g$ while calculating the radiative moments, since very little radiation is expected from a region very close to the horizon. The shock height is marked as $H_s = 0.6(x_s - 1)$ (Chakrabarti & Titarchuk 1995; Chattopadhyay 2005), therefore $\theta_{\text{ps}} = \tan^{-1}(x_s/H_s)$. The semi vertical angle of the SKD (θ_{sk} in Fig 1) is taken to be 85° . This assumption has been dictated by a large number of simulations, which showed SKD to have a flatter surface compared to PSD (Molteni *et al.* 1994, 1996; Giri & Chakrabarti 2013; Das *et. al.* 2014). The intercept of the SKD surface on the z-axis $d_0 = 0.4 \times H_s$. We chose $r_0 = 3500r_g$. SKD emits via synchrotron and bremsstrahlung processes, so the information of velocity (*i.e.*, density) and temperature profile is required, and have been estimated in appendix A. Injection speed (ϑ_0) for the SKD at the outer disc boundary is kept 0.001, the angular momentum of the disc λ is 1.7 and the temperature at $r = r_0$ is $\Theta_0 = 0.1$. The PSD is hotter than the rest of the disc (including SKD and KD) and puffs up in the form of a torus. KD emits thermal photons (Shakura & Sunyaev 1973) and SKD emits via bremsstrahlung and synchrotron processes. PSD emits bremsstrahlung and synchrotron photons, as well as, being fatter and hotter, inverse Comptonize these photons and the photons intercepted from SKD and KD to produce hard radiation. All the spectral states therefore, can be obtained by controlling the SKD accretion rate \dot{M}_{sk} and the KD accretion rate \dot{M}_{kd} . If \dot{M}_{kd} is relatively less than \dot{M}_{sk} , then due to the lack of supply of soft photons, PSD will remain hot, and thus producing the low hard or LH state. Increase in viscosity and/or increase in accretion rate at the outer boundary would push the shock closer to the central object (Kumar & Chattopadhyay 2013, 2014). This would brighten up the disc, but would make the spectra softer as the number of hard photons from the PSD would be lower due to the decrease in PSD size. Hence the spectral index would increase and spectra would enter the intermediate or IM states. The increased size of the pre-shock disc (SKD+KD) and the increased accretion rate, would eventually weaken the PSD or completely destroy it, the contribution of hard photons would plummet and the disc would be more luminous, while the spectra would become soft similar to a multicoloured black body.

2.2.1 Relativistic transformations of intensities from various disc components

In order to compute radiative moments, we need to know radiative intensities of various disc components. The intrinsic KD intensity is given by (Shakura & Sunyaev 1973)

$$I_{\text{kd}0} = \frac{3GM_B\dot{M}_{\text{kd}}}{8\pi^2r^3} \left(1 - \sqrt{\frac{3r_g}{r}}\right) \text{ erg cm}^{-2}\text{s}^{-1} \quad (17)$$

To compute the radiative moments from SKD, we need to know the temperature and density distribution of SKD, in order to calculate the intrinsic radiative intensity of SKD. The density and temperature of SKD starting with some outer boundary condition can only be solved numerically. However for simplicity, we estimate the approximate values of velocity, density and temperature profile of SKD in order to compute the $I_{\text{sk}0}$. Equations (A1, A3) give the analytical expression of all the components of three-velocities and the corresponding Lorentz factors (Appendix A) of the SKD. This allows us to compute the density profile for a given \dot{M}_{sk} . The density and temperature profile of SKD are estimated in equations (A6 & A7) in Appendix A1.

We further assume that there is stochastic magnetic field in the SKD which is in partial equipartition with the gas pressure. The ratio of magnetic pressure (p_{mag}) and the gas pressure (p_{gas}) is also assumed to be constant β *i.e.*, $p_{\text{mag}} = B^2/8\pi = \beta p_{\text{gas}} = \beta n_{\text{sk}}kT_{\text{sk}}$, where, n_{sk} and T_{sk} are the SKD local number density and temperature, respectively. The emission mechanism is dominated by synchrotron and bremsstrahlung emission, and therefore the SKD intensity is given by (Svensson 1982; Shapiro & Teukolsky 1983; Kumar *et al.* 2014; Kumar & Chattopadhyay 2014)

$$I_{\text{sk}0} = I_{\text{syn}} + I_{\text{brem}} \\ = \left[\frac{16}{3} \frac{e^2}{c} \left(\frac{eB_{\text{sk}}}{m_e c} \right)^2 \Theta_{\text{sk}}^2 n_{\text{sk}} r + 1.4 \times 10^{-27} n_{\text{sk}}^2 g_b c \sqrt{\frac{\Theta_{\text{sk}} m_e}{k}} \right] \frac{(d_0 \sin\theta_{\text{sk}} + r \cos\theta_{\text{sk}})}{3} \text{ erg cm}^{-2}\text{s}^{-1} \quad (18)$$

where, Θ_{sk} , n_{sk} , r , θ_{sk} , d_0 , B_{sk} and g_b are the pre-shock local dimensionless temperature, electron number density, horizontal distance from center of the disc, angle from the axis of symmetry to the pre-shock surface, the intercept of the SKD surface on to the axis of symmetry, the magnetic field and relativistic Gaunt factor ($g_b = 1 + 1.78\Theta^{1.34}$), respectively. The factor outside square brackets serves as the conversion factor from emissivity ($\text{erg.cm}^{-3}\text{s}^{-1}$) into intensity ($\text{erg.cm}^{-2}\text{s}^{-1}$).

The expression of intensity is more complicated for PSD, as a result we make further simplifying assumptions. The PSD itself emits via bremsstrahlung and synchrotron, but also

inverse Comptonizes its own photons, as well as, photons intercepted from SKD and KD. It is beyond the scope of this paper to do a proper radiative transfer treatment of the accretion disc. Instead, we fed the code of Mandal & Chakrabarti (2008) with the viscous and dissipative solutions of Kumar & Chattopadhyay (2014) as back ground solution, and computed the spectra from PSD, SKD and KD. The shock location x_s is estimated from equation B1 and is also presented in Fig. B(a). Although the relation between x_s and \dot{M}_{sk} has been obtained by generalizing the solutions for a certain viscosity parameter (Kumar & Chattopadhyay 2014), but we treat them as generic, since the general pattern is similar for a large number of cases we have analyzed. Then we fit the ratio of the luminosities of PSD and that from the pre-shock disc (SKD and KD) χ , as a function of x_s from the spectra obtained by the radiative transfer of the background solutions. The relation between χ and x_s is given by equations B4, B3 and is also plotted in Fig. B(b). The preshock luminosities are obtained by integrating I_{sk} and I_{kd} over the respective disc surfaces. So in principle we have two free parameters to fix the radiation field above the accretion disc, \dot{M}_{sk} and \dot{M}_{kd} . The intensity as measured in local rest frame of PSD is given by

$$I_{ps0} = L_{ps}/\pi A_{ps} = \ell_{ps} L_{Edd}/\pi A_{ps} \text{ (ergcm}^{-2}\text{s}^{-1}\text{)}, \quad (19)$$

where L_{ps} and A_{ps} are the PSD luminosity and the surface area of the PSD respectively. L_{Edd} is the Eddington luminosity and ℓ_{ps} is the PSD luminosity in units of L_{Edd} .

The intensities from either the PSD or SKD or KD components of the disc, namely, I_{ps0} , I_{sk0} and I_{kd0} , are measured in the local rest frames of the disc components. However, the matter in the disc is moving, so one has to transform the quantities into the observer frame! The intensity measured in the observer frame is presented in compact notation as,

$$I_j = \frac{I_{j0}}{\gamma_j^4 [1 + v_i l^i]_j^4} \quad (20)$$

Here γ_j is Lorentz factor and v^i is i^{th} component of 3-velocity of accreting matter and l^i s are directional cosines. The suffix $j \rightarrow ps, sk, kd$ signifies the contribution from either PSD, or SKD, or KD. For PSD and SKD v^i is calculated following Appendix A, while for KD $v^i \equiv (0, v_{kd}, 0)$ is the Keplerian azimuthal velocity. The luminosity from various components of the disc is obtained by integrating the respective local specific intensities over the disc surface *i.e.*,

$$L_j = 2 \int I_j \times 2\pi r \csc^2 \theta_j \, dr. \quad (21)$$

here, j represents various disc components. To compute the luminosity, the limits of integration are inner and outer limits of the disc components, for example for PSD the limit of integration is $r_{\text{in}} \rightarrow x_s$, while for SKD and KD the integration limits are $x_s \rightarrow r_0$. Apart from integration limits, various disc components are identified by the respective θ_{js} , which defines the surface of disc components. The total luminosity is given by $L = L_{\text{ps}} + L_{\text{sk}} + L_{\text{kd}}$, and in units of Eddington limit it is $\ell = \ell_{\text{ps}} + \ell_{\text{sk}} + \ell_{\text{kd}}$. All the transformations presented above, are exactly correct in the special relativistic regime. We are not taking into consideration the phenomenon of light bending since the jet spans from close to the horizon to few thousands of r_g . Beyond few tens of r_g the general relativistic effect may be ignored, but special relativistic effects cannot be. But close to the horizon, if only special relativistic effects are considered then the I_{ps} gets unnecessarily jacked up (Chattopadhyay 2005). In order to address this, we estimate the fraction of radiation that will not be absorbed by the black hole and escape. From geodesic equations of photons, it can be easily shown that if $\sin\psi > 3\sqrt{3}(1 - 1/\varpi)/(2\varpi)$ then the photon escapes (Shapiro & Teukolsky 1983), where ψ is the angle of the direction of propagation of light with the radial direction, and the ϖ is the spherical radius coordinate. So we express ψ in terms of r and θ_{ps} the semi vertical angle of the PSD inner surface. Assuming locally the radiation is isotropic, then the fraction of intensity from PSD which would escape and interact with the jet is,

$$\mathcal{R} = \frac{\pi - \sin^{-1}\left(3\sqrt{3}(\sin\theta_{\text{ps}}/2r)(1 - \sin\theta_{\text{ps}}/r)\right)}{\pi} \quad (22)$$

Since SKD and KD is further away from the black hole, no such estimation of gravity effect on emitted radiation from these components is needed.

2.2.2 Computation of radiative moments

Radiative moments are the zeroth, first and second moments of specific intensity, and frequency integrated moments are respectively called radiation energy density, radiative flux and radiation pressure, and are expressed as following,

$$\begin{pmatrix} E \\ F^i \\ P^{jk} \end{pmatrix} = \int \int \begin{pmatrix} \frac{1}{c} \\ l^i \\ \frac{l^j l^k}{c} \end{pmatrix} I_\nu d\nu d\Omega$$

Here, l^i s are directional derivatives, ν the frequency of radiation and Ω is the solid angle subtended by the field point (where the moments are calculated) on to the source of radiation. Since we are considering on axis jet, therefore we need to compute the radiative moments

only along the axis. The radiative moments along the jet axis (z axis) are calculated from the PSD, SKD and KD components of this hybrid disc model, these components are indicated in following expressions with subscripts ps, sk and kd respectively.

$$\mathcal{E} = \frac{\sigma_T}{mc} \left(\int I_{\text{ps}} d\Omega_{\text{ps}} + \int I_{\text{sk}} d\Omega_{\text{sk}} + \int I_{\text{kd}} d\Omega_{\text{kd}} \right) = \frac{\sigma_T}{m} (E_{\text{ps}} + E_{\text{sk}} + E_{\text{kd}}) \\ = \mathcal{E}_{\text{ps}} + \mathcal{E}_{\text{sk}} + \mathcal{E}_{\text{kd}} \quad (23)$$

$$\mathcal{F} = \frac{\sigma_T}{mc} \left(\int I_{\text{ps}} l^z d\Omega_{\text{ps}} + \int I_{\text{sk}} l^z d\Omega_{\text{sk}} + \int I_{\text{kd}} l^z d\Omega_{\text{kd}} \right) = \frac{\sigma_T}{mc} (F_{\text{ps}} + F_{\text{sk}} + F_{\text{kd}}) \\ = \mathcal{F}_{\text{ps}} + \mathcal{F}_{\text{sk}} + \mathcal{F}_{\text{kd}} \quad (24)$$

$$\mathcal{P} = \frac{\sigma_T}{mc} \left(\int I_{\text{ps}} l^z l^z d\Omega_{\text{ps}} + \int I_{\text{sk}} l^z l^z d\Omega_{\text{sk}} + \int I_{\text{kd}} l^z l^z d\Omega_{\text{kd}} \right) = \frac{\sigma_T}{m} (P_{\text{ps}} + P_{\text{sk}} + P_{\text{kd}}) \\ = \mathcal{P}_{\text{ps}} + \mathcal{P}_{\text{sk}} + \mathcal{P}_{\text{kd}} \quad (25)$$

All the points on the axis of symmetry are field points (z), *i.e.*, where radiative moments are to be computed. The coordinates on the disc surface are r , ϕ , z' and $z'_j = r \cot\theta_j$, where $j \equiv \text{ps/sk/kd}$. It is easy to see that for extended source, and field point close to the source, the directional cosines of $l^z < 1$, but for point source $l^z = 1$, and $\mathcal{E} = \mathcal{F} = \mathcal{P}$. Therefore, according to the note following equation (15), for point sources $\mathfrak{R} = (\mathcal{E} + \mathcal{P})/2\mathcal{F} = 1$ and there will be no radiation drag. The radiative moments from PSD are,

$$\mathcal{E}_{\text{ps}} = \mathcal{S} \int_{r_{\text{in}}}^{x_s} \int_0^{2\pi} \frac{\mathcal{R} z r dr d\phi}{[(z - r \cot\theta_{\text{ps}})^2 + r^2]^{3/2} \gamma_{\text{ps}}^4 [1 + v_i l^i]_{\text{ps}}^4} \quad (26)$$

$$\mathcal{F}_{\text{ps}} = \mathcal{S} \int_{r_{\text{in}}}^{x_s} \int_0^{2\pi} \frac{\mathcal{R} z (z - r \cot\theta_{\text{ps}}) r d\phi dr}{[(z - r \cot\theta_{\text{ps}})^2 + r^2]^2 \gamma_{\text{ps}}^4 [1 + v_i l^i]_{\text{ps}}^4} \quad (27)$$

$$\mathcal{P}_{\text{ps}} = \mathcal{S} \int_{r_{\text{in}}}^{x_s} \int_0^{2\pi} \frac{\mathcal{R} z (z - r \cot\theta_{\text{ps}})^2 r d\phi dr}{[(z - r \cot\theta_{\text{ps}})^2 + r^2]^{5/2} \gamma_{\text{ps}}^4 (1 + v_i l^i)_{\text{ps}}^4} \quad (28)$$

\mathcal{S} is a constant, which is obtained after converting the whole expression in geometric units mentioned after equation 13,

$$\mathcal{S} = \frac{1.3 \times 10^{38} \ell_{\text{ps}} \sigma_T}{2\pi c m_e A_{\text{ps}} G M_{\odot}}$$

$\sigma_T, m_e, G, M_{\odot}, A_{\text{ps}}, \ell_{\text{ps}}$ are Thomson scattering cross section, rest mass of electron, constant of gravitation, solar mass, surface area of PSD and post shock luminosity in units of Eddington luminosity ($L_{\text{Edd}} = 1.3 \times 10^{38} M_B / M_{\odot}$) respectively. Now, depending on the central mass, ℓ_{ps} is calculated from equation (B3 or B4), and hence depends on SKD and KD accretion rates.

The radiative moments from the SKD are

$$\mathcal{E}_{\text{sk}} = \int_{r_{11}}^{r_0} \int_0^{2\pi} F_{\text{sk}} \frac{(r \cos \theta_{\text{sk}} + d_0 \sin \theta_{\text{sk}}) z dr d\phi}{r u_{\text{sk}}^2 (\cot \theta_{\text{sk}} r + d_0)^2 [(z - r \cot \theta_{\text{sk}})^2 + r^2]^{3/2} \gamma_{\text{sk}}^4 (1 + v_i l^i)_{\text{sk}}^4} \quad (29)$$

$$\mathcal{F}_{\text{sk}} = \int_{r_{11}}^{r_0} \int_0^{2\pi} F_{\text{sk}} \frac{(r \cos \theta_{\text{sk}} + d_0 \sin \theta_{\text{sk}}) z (z - r \cot \theta_{\text{sk}}) dr d\phi}{r u_{\text{sk}}^2 (\cot \theta_{\text{sk}} r + d_0)^2 [(z - r \cot \theta_{\text{sk}})^2 + r^2]^2 \gamma_{\text{sk}}^4 (1 + v_i l^i)_{\text{sk}}^4} \quad (30)$$

$$\mathcal{P}_{\text{sk}} = \int_{r_{11}}^{r_0} \int_0^{2\pi} F_{\text{sk}} \frac{(r \cos \theta_{\text{sk}} + d_0 \sin \theta_{\text{sk}}) z (z - r \cot \theta_{\text{sk}})^2 dr d\phi}{r u_{\text{sk}}^2 (\cot \theta_{\text{sk}} r + d_0)^2 [(z - r \cot \theta_{\text{sk}})^2 + r^2]^{5/2} \gamma_{\text{sk}}^4 (1 + v_i l^i)_{\text{sk}}^4} \quad (31)$$

With

$$F_{\text{sk}} = \mathcal{S}_{\text{ks}} \left(\frac{u_0 r_0 H_0}{u_{\text{sk}} r H} \right)^{3(\Gamma-1)} + \mathcal{S}_{\text{kb}} \left(\frac{u_0 r_0 H_0}{u_{\text{sk}} r H} \right)^{\frac{(\Gamma-1)}{2}} \left[1 + 1.78 \left\{ \Theta_0 \left(\frac{u_0 r_0 H_0}{u_{\text{sk}} r H} \right)^{(\Gamma-1)} \right\}^{1.34} \right] \quad (32)$$

Constants \mathcal{S}_{ks} and \mathcal{S}_{kb} are associated with synchrotron and bremsstrahlung terms and are given as

$$\mathcal{S}_{\text{ks}} = \frac{9.22 \times 10^{33} e^4 \Theta_0^3 \beta \sigma_T \dot{m}_{\text{sk}}^2}{\pi m_e^2 m_{p^+}^2 c^2 G^2 M_\odot^2}$$

$$\mathcal{S}_{\text{kb}} = \frac{1.51 \times 10^5 \dot{m}_{\text{sk}}^2 \sqrt{\Theta_0} \sigma_T}{\pi^2 m_{p^+}^2 M_\odot^2 G^2 \sqrt{m_e k}}$$

Here $\dot{m}_{\text{sk}} = \dot{M}_{\text{sk}} / \dot{M}_{\text{Edd}}$, where the Eddington accretion rate $\dot{M}_{\text{Edd}} = 1.44 \times 10^{17} (M_B / M_\odot) \text{ g s}^{-1}$ and $L_{\text{Edd}} = \dot{M}_{\text{Edd}} c^2$. From a certain point z on the axis, due to the shadow effect of the PSD the inner edge of SKD observed is given by

$$r_{11}(z) = \frac{z - d_0}{(z - H_s) / x_s + \cot \theta_{\text{sk}}}$$

Therefore, to obtain the radiative moments at some z on the jet axis the integration limit on r is r_{11} to r_0 .

Similarly from KD, the moments are

$$\mathcal{E}_{\text{kd}} = \mathcal{K} \int_{r_{12}}^{r_0} \int_0^{2\pi} \frac{z(r^{-2} - \sqrt{3}r^{-5/2}) d\phi dr}{(z^2 + r^2)^{3/2} \gamma_{\text{kd}}^4 (1 + v_i l^i)_{\text{kd}}^4} \quad (33)$$

$$\mathcal{F}_{\text{kd}} = \mathcal{K} \int_{r_{12}}^{r_0} \int_0^{2\pi} \frac{z(r^{-2} - \sqrt{3}r^{-5/2}) d\phi dr}{(z^2 + r^2)^2 \gamma_{\text{kd}}^4 (1 + v_i l^i)_{\text{kd}}^4} \quad (34)$$

$$\mathcal{P}_{\text{kd}} = \mathcal{K} \int_{r_{12}}^{r_0} \int_0^{2\pi} \frac{z(r^{-2} - \sqrt{3}r^{-5/2}) d\phi dr}{(z^2 + r^2)^{5/2} \gamma_{\text{kd}}^4 (1 + v_i l^i)_{\text{kd}}^4} \quad (35)$$

The shadow effect of blocking a fraction of radiation from the KD by the PSD is also taken into account and the integration is done from r_{12} and is given by

$$r_{12}(z) = \frac{x_s z}{z - H_s},$$

and the dimensionless constant \mathcal{K} is given by

$$\mathcal{K} = \frac{4.32 \times 10^{17} \dot{m}_{\text{kd}} \sigma_T c}{32 \pi^2 m_e G M_\odot},$$

with \dot{m}_{kd} being the Keplerian accretion rate in units of \dot{M}_{Edd} .

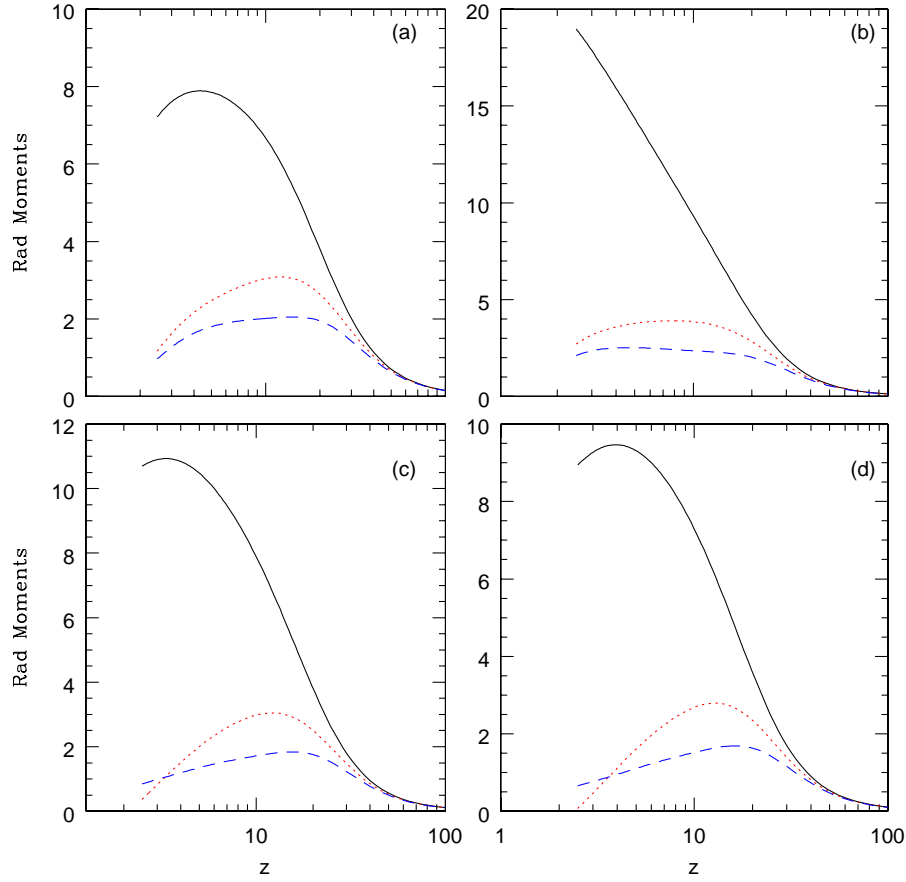


Figure 2. Distribution of radiative moments from the post-shock disc (PSD) with z (in units of r_g). Each curve represents $\mathcal{E}_{\text{ps}}/\mathcal{S}$ (solid, black online), $\mathcal{F}_{\text{ps}}/\mathcal{S}$ (dotted, red online) and $\mathcal{P}_{\text{ps}}/\mathcal{S}$ (dashed, blue online), respectively. Various panels are for radiative moments (a) without relativistic transformations in the accretion disc, (b) with special relativistic transformations up to first order in v , (c) with full special relativistic transformations and (d) with approximate general relativistic correction and full special relativistic transformations. All the figures are obtained for $\dot{m}_{\text{sk}} = 5.06$, which produces a shock at $x_s = 20$ around a $10M_{\odot}$ BH.

2.2.3 Nature of radiative moments

We now numerically integrate equations (26-35) to obtain the radiative moments from PSD, SKD, and KD. In Fig. 2a-d we present a comparative study of the space dependent part of the radiative moments *i.e.*, $\mathcal{E}_{\text{ps}}/\mathcal{S}$ (solid, black online), $\mathcal{F}_{\text{ps}}/\mathcal{S}$ (dotted, red online) and $\mathcal{P}_{\text{ps}}/\mathcal{S}$ (dashed, blue online) from PSD which were computed in previous works and the present one, because we would like to show the effect of various corrections considered, while computing the radiative moments. To compare the moments from PSD, we need to know the size of PSD. This is obtained by estimating the x_s from the supplied \dot{m}_{sk} . For $\dot{m}_{\text{sk}} = 5.06$, we estimate $x_s = 20$ (equation B1). Figure 2(a) presents the radiative moments from PSD when the accretion disc was treated as a simple radiator without any dynamics (Chattopadhyay *et al.* 2004). In Fig. 2(b), we applied special relativistic transformations while computing the intensities in the observer frame from the local disc frame, but the Lorentz factor (γ_j) in

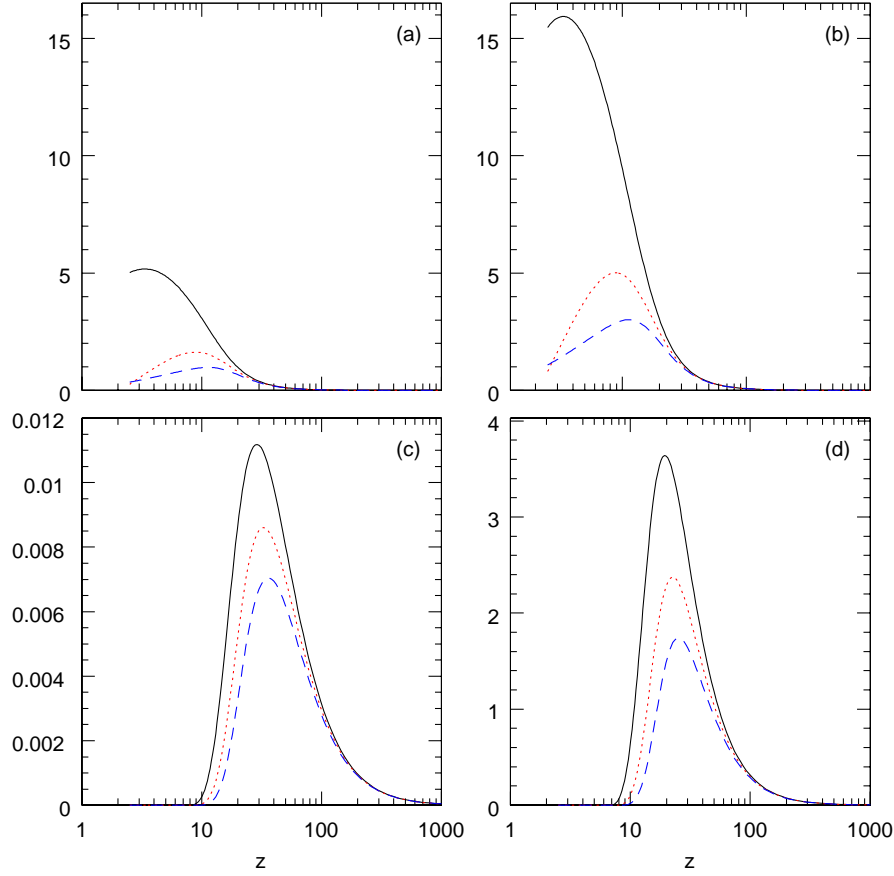


Figure 3. Distribution of radiative moments \mathcal{E} (solid, online black), \mathcal{F} (dotted, online red) and \mathcal{P} (dashed, online blue) from PSD for (a) $10M_{\odot}$ and (b) 10^8M_{\odot} black holes. Distribution of radiative moments from the Kd (c) and from SKD (d) is same for both types of black holes when expressed in the geometric units. Various parameters used to compute the moments are $\dot{m}_{\text{sk}} = 7$, $\dot{m}_{\text{kd}} = 1$ and $\beta = 0.5$. This produce $x_s = 13.2032$ and luminosities are $\ell_{\text{sk}} = 0.0265$, $\ell_{\text{kd}} = 0.039$ and for stellar mass BH $\ell_{\text{ps}} = 0.215$ (a), while for larger BH $\ell_{\text{ps}} = 0.661$ (b).

the red-shift factor of the intensity (equation 20) was ignored (Chattopadhyay 2005). And in Fig. 2(c) we show moments computed with correct special relativistic transformations. Figure 2(d) shows only the distribution of space dependent part of radiative moments from PSD which is being used in the current study. In this panel, moments are with full special relativistic transformations and general relativistic correction for the radiation absorbed by the black hole near horizon. We notice that general relativistic correction (Fig. 2d) reduces the absolute value of the moments and the moments peak at a slightly different location on the axis than the previous case (Fig. 2c). Ignoring the effect of disc motion while computing radiative moments, under-estimates the moments (Fig. 2a), while partial implementation of the very effect, over estimates the radiative moments (Fig. 2b) to unrealistic values. In this paper, we use full special relativistic transformation and general relativistic corrections for the radiative moments from PSD (as in Fig. 2d).

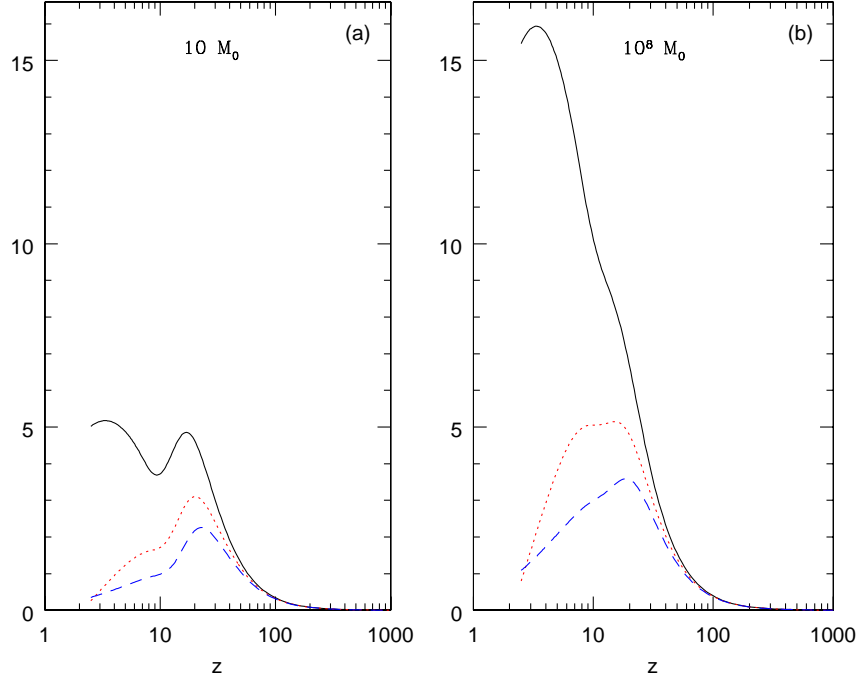


Figure 4. Combined moments from (a) 10 and (b) $10^8 M_\odot$ black holes. Various curves are \mathcal{E} (solid, online black), \mathcal{F} (dashed, online red) and \mathcal{P} (dashed, online blue). Disc parameters are $\dot{m}_{\text{sk}} = 7$ and $\dot{m}_{\text{kd}} = 1$, $\beta = 0.5$ for which the shock obtained is at $x_s = 13.2032$, luminosities are $\ell_{\text{sk}} = 0.0265$, $\ell_{\text{kd}} = 0.039$. The $\ell_{\text{ps}} = 0.215$ for $10 M_\odot$ BH and $\ell_{\text{ps}} = 0.661$ for $10^8 M_\odot$ BH. The moments are expressed in geometric units.

From Appendix B1, it is clear that ℓ_{ps} is different for $10 M_\odot$ and $10^8 M_\odot$ BH, for the same set of free parameters *i.e.*, \dot{m}_{sk} and \dot{m}_{kd} . This should affect the net radiation field above the disc. In Fig. 3a, we plot \mathcal{E}_{ps} (solid, black online), \mathcal{F}_{ps} (dotted, red online) and \mathcal{P}_{ps} (dashed, blue online) with z for $\dot{m}_{\text{sk}} = 7$ and $\dot{m}_{\text{kd}} = 1$ for $M_B = 10 M_\odot$. For such accretion rate the shock is at $x_s = 13.203$ (see, equation B1). In Fig. 3b, we plot radiative moments above a disc around a $M_B = 10^8 M_\odot$ BH, for the same set of accretion parameters. The radiative moments from the PSD around $10^8 M_\odot$ BH are about three times than those around $10 M_\odot$. It may be noted, that for lower \dot{m}_{sk} the shocks are formed at larger distance away from the BH, and the radiative moments around stellar mass and super-massive BH are same. In Fig. 3c, we plot \mathcal{E}_{kd} (solid, black online), \mathcal{F}_{kd} (dotted, red online) and \mathcal{P}_{kd} (dashed, blue online). In Fig. 3d we present \mathcal{E}_{sk} (solid, black online), \mathcal{F}_{sk} (dotted, red online) and \mathcal{P}_{sk} (dashed, blue online). The PSD luminosity for $10 M_\odot$ BH is about $\ell_{\text{ps}} = 0.215$ and $\ell_{\text{ps}} = 0.661$ for $10^8 M_\odot$ BH. The luminosities of the pre-shock disc $\ell_{\text{sk}} = 0.0265$ and $\ell_{\text{kd}} = 0.039$ are same for

discs around super massive, as well as, stellar mass BH. The moments due to PSD around a super-massive BH is larger than that around stellar mass BH, however, the SKD and KD contributions in the geometric units are exactly same for stellar mass and super massive BH. In physical units these moments would scale with the central mass. Finally, we show combined radiative moments from all the disc components for $10M_{\odot}$ (Fig. 4a) and 10^8M_{\odot} BH (Fig. 4b) for exactly the same disc parameters as in Fig. 3a-d. For higher \dot{m}_{sk} , the overall radiation field (in geometric units), above a disc around a stellar mass BH is different than the moments around a super massive BH. This is because the for higher \dot{m}_{sk} the shock in accretion is located closer to the BH, which produces a cooler PSD around a stellar mass BH than a super massive BH and therefore, larger efficiency of Comptonization. However, for lower \dot{m}_{sk} (equation B1 & Fig. A1a), the shock is located at larger distance from the BH, and the efficiency of Comptonization is similar for both kinds of BH, and hence the moments are similar too.

3 SOLUTION METHOD

To obtain the solution of steady state, relativistic jet, we need to integrate equations (14) and (15) simultaneously. Alternatively, one may integrate equation (15) with the help of equation (13), since equation (13) is the integrated version of equation (14). We employ Runge-Kutta's 4th order method to integrate differential equations.

3.1 Sonic point conditions

Since jets originate from a region in the accretion disc, close to the central object, the base jet velocity should be small. However due to this proximity of the jet base to the central object, the temperatures at the jet base should be very high. In other words, jets are subsonic at its base. While far away from the central object the thermal energy and the radiative energy would drive jets to large v , but simultaneously becoming less hot, *i.e.*, outer boundary condition of the jet is super sonic. This means at some point the jet would become transonic, and the point in which this happens is called the sonic point z_c and the derivative $dv/dz \rightarrow 0/0$ (eq. 15). This gives us the so-called sonic point conditions,

$$v_c = a_c$$

$$a_c^2 = \frac{z_c}{2\gamma_c^2} \left[\frac{1}{2(z_c - 1)^2} - \frac{\gamma_c^2 \tau}{f_c + 2\Theta_c} \left\{ (1 + v_c^2) \mathcal{F}_c - v_c (\mathcal{E}_c + \mathcal{P}_c) \right\} \right]. \quad (36)$$

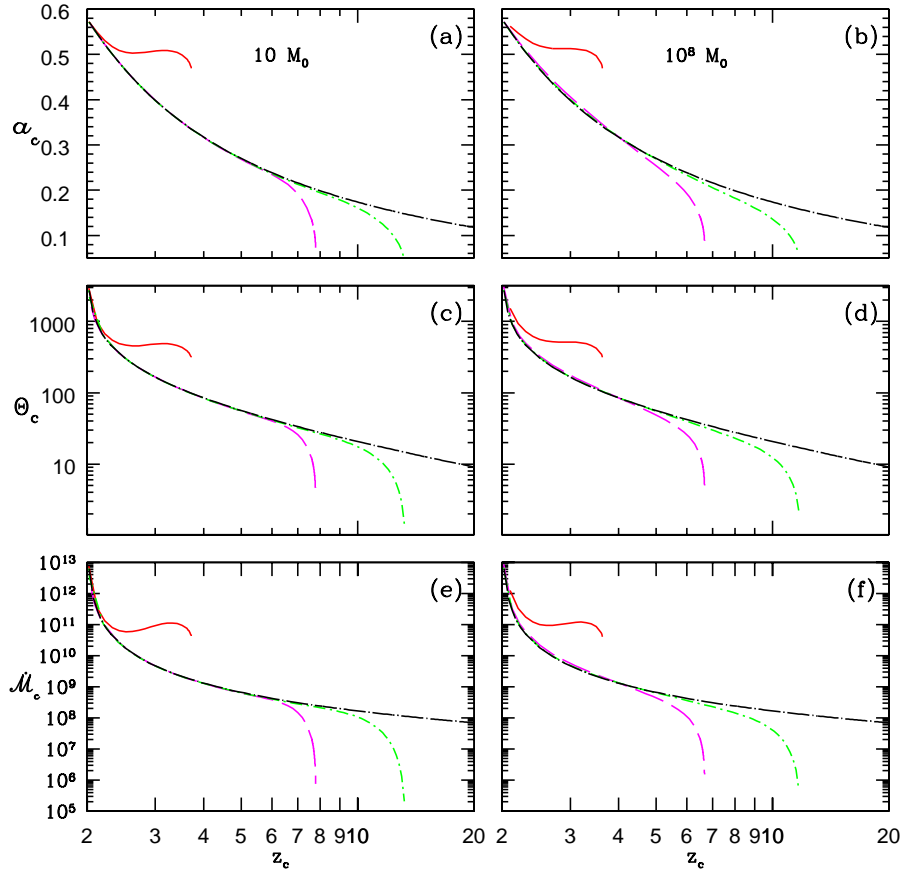


Figure 5. Variation of a_c (a, b), Θ_c (c, d) and $\dot{\mathcal{M}}_c$ (e, f) as a function of z_c for jets are around $M1 = 10M_\odot$ BH (a, c, e) and $M8 = 10^8 M_\odot$ BH (b, d, f). Each curve corresponds to $\dot{m}_{\text{sk}} = 13$ (solid, red online), 10 (long dashed, magenta online), 8 (dashed-dotted, green online), and only thermally driven jet (long-dashed dotted, black online). For all the plots $\dot{m}_{\text{kd}} = 1$.

The $dv/dz|_c$ is calculated by employing the L'Hospital's rule at z_c and solving the resulting quadratic equation of $dv/dz|_c$. The resulting quadratic equation can admit two complex roots leading to the so-called O type or 'centre' type sonic points, or two real roots. The solutions with two real roots but with opposite signs are called X or 'saddle' type sonic points, while real roots with same sign produces the nodal type sonic point. The jet solutions flowing through X type sonic points are physical, and in this paper care has been taken to study jet solutions through X type sonic points. So for a given set of flow variables at the jet base, a unique solution will pass through the sonic point determined by the entropy $\dot{\mathcal{M}}$ of the flow. For given values of inner boundary condition *i.e.*, at the jet base z_b , v_b and a_b , we integrate equation (15) and (14), while checking for the sonic point conditions (equations 36). We iterate till the sonic point is obtained, and once it is obtained we continue to integrate outwards starting from the sonic point. From equation (36) it is clear that for a thermally driven jet, sonic point exists from $z_c = 2 \rightarrow \infty$. However, radiatively driven flow

may not possess sonic point at large distances away from the jet base, because the presence of strong radiation field may render $a_c \lesssim 0$ at those distances. In Figs. 5a-f, we compare the flow quantities a_c (a, b), Θ_c (c, d), $\dot{\mathcal{M}}_c$ (e, f) as a function of z_c . The left panels show the sonic point properties of jets around $10M_\odot$ BH (a, c, e) and the right panels show sonic point properties of jets around 10^8M_\odot BH (b, d, f). The KD accretion rate, or, $\dot{m}_{\text{kd}} = 1$ is kept invariant for all these plots, but various curves are for $\dot{m}_{\text{sk}} = 13$ (solid, red online), 10 (long dashed, magenta online), 8 (dashed-dotted, red online), and only thermally driven jet (long-dashed dotted, black online). It is interesting to note that, the region outside the central object available for sonic points shrinks, as the disc luminosity increases. For luminous discs say $\dot{m}_{\text{sk}} > 10$, sonic points can only form for $z_c < 8$. This implies that only very hot flow has thermal energy density comparable to the radiation pressure, and therefore for any flow with less thermal energy may be considered as collection of particles rather than a fluid in such radiation field. Moreover, for $\dot{m}_{\text{sk}} = 13$, multiple sonic points may form for some values of $\dot{\mathcal{M}}$.

4 RESULTS

A radiatively inefficient disc can only give rise to thermally driven jets and not radiatively driven jets, so we choose luminous disc. We discuss the jet properties for electron-proton jets *i.e.*, $\xi = 1$, until specified otherwise. We choose $\dot{m}_{\text{kd}} = 1$ to generate the KD radiative moments until specified otherwise. The accreting material is assumed to possess stochastic magnetic field with constant magnetic to gas pressure ratio $\beta = 0.5$, until specified otherwise. In Fig. 6a, we plot the jet 3-velocity v (solid, black online) and the sound speed a (dashed dotted, blue online) as a function of z . This jet is from a disc around a stellar mass BH. The sonic point z_c is at the crossing point of v and a . The terminal speed achieved for this case is $v_T \sim 0.45$, and the total disc luminosity is $\ell = \ell_{\text{ps}} + \ell_{\text{sk}} + \ell_{\text{kd}} \sim 0.14$ in units of L_{Edd} . In Fig. 6b we plot $\dot{\mathcal{M}}$ as a function of z and in Fig. 6c we plot the variation of Γ or adiabatic index of the jet. The inner boundary condition is $z_b = 1.5r_g$, $v_b = 0.014$ and $a_b = 0.51$, and the SKD and the KD accretion rates are $\dot{m}_{\text{sk}} = 5$ and $\dot{m}_{\text{kd}} = 1$. Since the interaction between radiation and the jet material is assumed to be in the Thompson scattering regime, the source term of the first law of thermodynamics turns out to be zero (*i.e.*, equation 14), and therefore $\dot{\mathcal{M}}$ which is a measure of entropy, remains constant through out the flow. The base of the jet is very hot, therefore $\Gamma \rightarrow 4/3$ at the base. However, as the jet expands to relativistic

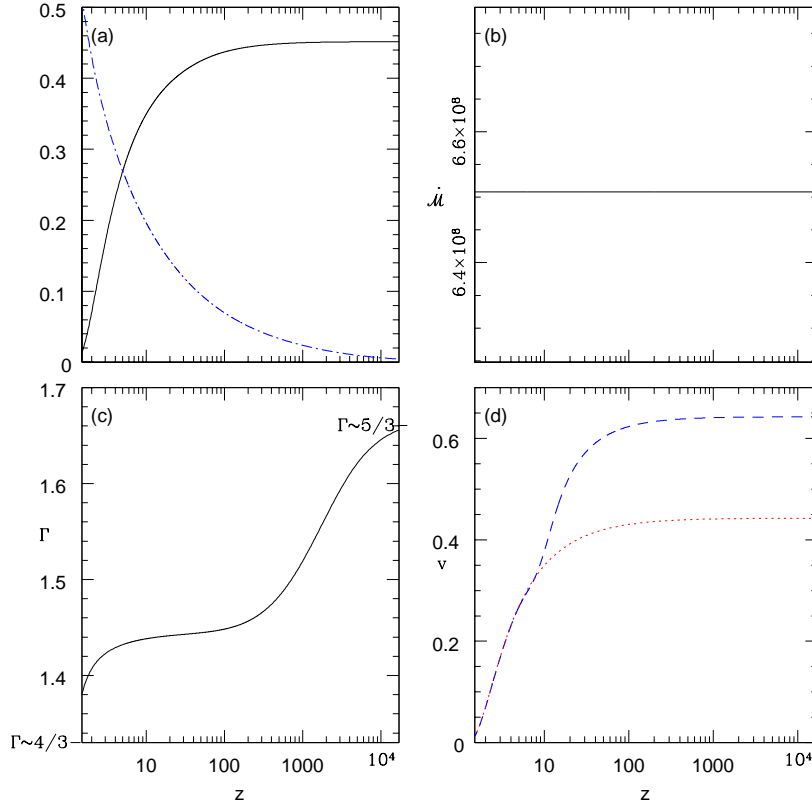


Figure 6. (a) The variation of jet 3-velocity v (solid, black online) and sound speed a (dashed-dotted, blue online) with z . (b) \mathcal{M} is plotted as a function of z and (c) the variation of Γ with z . All the plots are generated for inner boundary condition $z_b = 1.5$, $v_b = 0.014$ and $a_b = 0.51$, and the SKD and the KD accretion rates are $\dot{m}_{sk} = 5$ and $\dot{m}_{kd} = 1$, $\beta = 0.5$ and shock obtained is at $x_s = 20.27r_g$ and luminosities are $\ell_{sk} = 0.0082$, $\ell_{ps} = 0.113$, $\ell_{kd} = 0.027$. (d) Comparison of v for a thermally driven jet (dotted, red online) and radiatively plus thermally driven jet (dashed, blue online). Here accretion parameters are $\dot{m}_{kd} = 1$, $\beta = 0.5$ and $\dot{m}_{sk} = 10$ for the radiatively and thermally driven jet. For thermally driven flow no radiation interaction has been considered. The luminosities are $\ell_{sk} = 0.108$, $\ell_{kd} = 0.055$ and $\ell_{ps} = 0.38$. The composition of the jet is $\xi = 1$ or $e^- - p^+$ plasma, and is launched around a $10M_\odot$ BH.

velocities (at $z \rightarrow \text{large}$), the temperature falls such that $\Gamma \rightarrow 5/3$. In Fig. 6d, we compare the v profile of a thermally driven jet (dotted, red online) with a radiatively plus thermally driven jet (dashed, blue online) starting with the same base values. The radiatively driven fluid jet (blue dashed) is powered by radiation from a disc with parameters $\dot{m}_{sk} = 10$ and $\dot{m}_{kd} = 1$. From the base to first few r_g , the v profiles of the two flows are almost identical, and the radiative driving is perceptible at $z > 7.66$. The terminal speed of the thermally driven flow is slightly less than 0.45 and for the radiatively driven flow it is $v_T \lesssim 0.65$. The radiative driving of the jet is ineffective in regions close to the z_b , because the thermal driving accelerates the jet to $v \sim v_{eq}$. Therefore radiative driving is ineffective in those region, and results in a similar v profile up to $z \sim 7.66$, but beyond it radiative driving generates a flow with a 44% increase in v_T .

In Fig. 7a-b, we show a transonic jet from a disc around a stellar mass BH, in which,

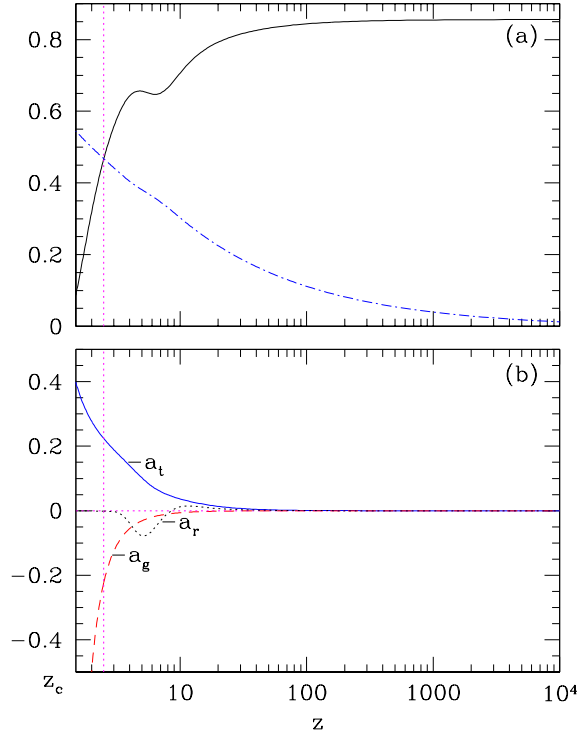


Figure 7. (a) Variation of v (solid, online black) and a (dashed-dotted, online blue), The base speed $v_b = 0.087$ and sound speed $a_b = 0.545$ at jet base $z_b = 1.5r_g$, critical point obtained is at $z_c = 2.5r_g$; (b) Variation of a_t (solid, blue online), a_r (dotted, black online) and a_g (dashed, red online) with z . The SKD and the KD accretion rates are $\dot{m}_{sk} = 12$ and $\dot{m}_{kd} = 1$, $\beta = 0.5$ and shock obtained is at $x_s = 5.87$ and luminosities of various disc components around $10M_\odot$ BH, are $\ell_{sk} = 0.295$, $\ell_{ps} = 0.522$ and $\ell_{kd} = 0.0667$. The composition of the jet is $\xi = 1$. The vertical dashed line (magenta online) shows the position of sonic point z_c .

the jet has been accelerated, as well as, decelerated by radiation. In Fig. 7a, we plot v (solid, black online) and a (dotted dashed, blue online) as a function of z for inner boundary condition $v_b = 0.087$, $a_b = 0.545$ at $z_b = 1.5$, and $\dot{m}_{sk} = 12$ and $\dot{m}_{kd} = 1$. In this case the sonic point is obtained at $z_c = 2.5$. The total luminosity turns out to be $\ell = 0.884$. The 3-velocity v increases beyond z_c and up to $z \sim 4$, and then decelerates in the region $4 < z \lesssim 7$ and thereafter again accelerates till it reaches terminal value at $v_T \sim 0.86$. Let us analyze the various terms that influence v . In Fig. 7b, we plot the variation of gravitational acceleration term or a_g (dashed, red online), the radiative term a_r (dotted, black online), and acceleration due to thermal driving a_t (solid, blue online). In both the panels the dashed vertical line (magenta online) shows the location of z_c . From the l. h. s of equation (15), it is clear that in the subsonic region v can increase (*i.e.*, jet accelerate) with z only if r. h. s is negative. While in the supersonic region the jet accelerates if the r. h. s is positive. The gravity term or a_g is always negative, while a_t is always positive. In this particular solution $a_r < 0$ for $z < 8.53$. In the sub sonic region *i.e.*, $z < z_c$, $|a_r| \ll a_t$ and $a_t < a_g$, therefore r. h. s of equation (15) is negative and the jet is accelerated. At the sonic point $a_t = a_g + a_r$. For

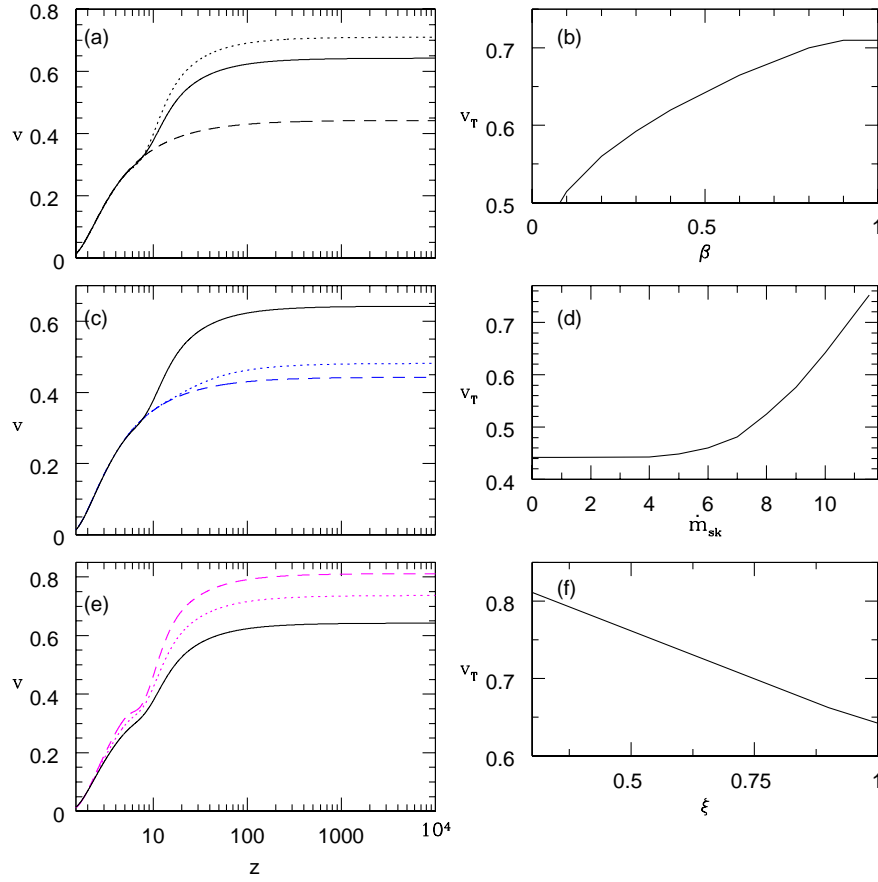


Figure 8. (a) Variation of v with z . Each curve represents $\beta = 1.0$ (dotted, black online), 0.5 (solid, black online) and 0.0 (dashed, black online). (b) Variation of v_T with β . Other parameters same as (a). (c) Variation of v with z . Each curve represents $\dot{m}_{sk} = 1.0$ (dashed, blue online), 7 (dotted, blue online) and 10 (solid, black online). (d) Variation of v_T with \dot{m}_{sk} . Other parameters same as (c). (e) Variation of v with z . Each curve represents $\xi = 1.0$ (solid, black online), 0.6 (dotted, magenta online) and 0.3 (dashed, magenta online). (f) Variation of v_T with ξ . Other parameters same as (e). Accretion parameters are $\dot{m}_{sk} = 10$ (in a, b, e, f), $\beta = 0.5$ (in c, d, e, f), $\xi = 1.0$ (in a, b, c, d) and $\dot{m}_{kd} = 1$. Jet base values are $z_b = 1.5$, $v_b = 0.014$ and $a_b = 0.51$. The mass of central black hole is $10M_\odot$.

$z > z_c$, a_r decreases to its minimum value at $z = 5.15$. Gravity is less important at these distances and $a_r \gtrsim a_t$, which makes the r. h. s negative. Therefore, the jet decelerates in the range $4.78 < z < 6.34$. For $z > 6.34$, $|a_r|$ decreases, ultimately becomes positive, making r.h.s to be positive again. So the jet starts to accelerate at $z > 6.34$ until $v \rightarrow v_T$.

Now we discuss how various disc parameters and fluid composition of the jet affect dynamics of the jet. The jet is being affected by the radiation from the disc, and the radiation field above the disc is influenced by β , \dot{m}_{sk} , and \dot{m}_{kd} . The base values of the jet are $v_b = 0.014$ and $a_b = 0.51$ at $z_b = 1.5$. In Fig. 8a we show the comparison of v as a function of z for various values of $\beta \rightarrow 0.0$ (dashed, black online), 0.5 (solid, black online) and 1.0 (dotted, black online). The corresponding terminal speeds (v_T) at $z = 10^4$ with β are presented in Fig. 8b. As the magnetic pressure increases in the disc *i.e.*, β increases, the supersonic part

of the jet is accelerated because ℓ_{sk} increases. When magnetic pressure is zero ($\beta = 0.0$) *i.e.*, the jet is thermally and radiatively driven only by pre-shock bremsstrahlung and thermal photons, the terminal speed is at around 0.44. And when magnetic pressure is taken to be equal to the gas pressure, then v_T increases above 0.7. In Fig. 8c we show the effect of accretion rate of SKD on the v profile and the corresponding terminal speeds are presented in Fig. 8d as a function of \dot{m}_{sk} . We see that v_T ranges from 0.42 to 0.72 when the \dot{m}_{sk} is varied from 0.1 to 11.5. The velocity profile of a thermally driven jet, and a jet driven by radiations acted on by $\dot{m}_{\text{sk}} = 1$ is similar. Only when the luminosity is close to L_{Edd} of $\ell \rightarrow 1$, the radiative driving is significant. In Fig. 8e we carry out similar analysis for the variation of composition parameter (ξ) in the jet, and plot v profiles for jet with $\xi = 0.3$ (dashed, magenta online), 0.5 (dotted, magenta online) and 1.0 (solid, black online). With the lighter jet v increases, and this is also seen in the v_T dependence of ξ in Fig. 8f. As ξ increases, high proton fraction makes the jet heavier per unit pair of particles, and the optical depth decreases due to the decrease in total number of leptons. So the net radiative momentum deposited on to the jet per unit volume decreases, in addition the inertia also increases. This makes the jets with higher ξ to be slower.

For various values of \dot{m}_{sk} , x_s changes and therefore not only ℓ_{sk} changes but ℓ_{ps} changes too. Infact since x_s is the inner edge of the KD, ℓ_{kd} will change even though \dot{m}_{kd} is kept constant. In Fig. 9a, we plot v_T with the total luminosity ℓ ($\equiv \ell_{\text{ps}} + \ell_{\text{sk}} + \ell_{\text{kd}}$), by tuning \dot{m}_{sk} . As the luminosity of the disc increases the terminal speed increases from moderate values of 0.44 to high speeds of ~ 0.8 when the disc luminosity is closer to Eddington limit. However, ℓ_{kd} has limited role in determining v_T as has been shown in Fig. 9b.

In Fig. 4 the radiative moment around a super-massive BH is shown to be significantly higher than that around a stellar mass BH even if the accretion rates (in units of \dot{M}_{Edd}) are same. In order to study the effect of the mass of the central object, in Fig. 10a, we compare the v profile of the jet around $10M_{\odot}$ BH (solid, black online) with that around 10^8M_{\odot} BH (dotted, blue online). The jets are launched with the same base values ($z_b = 1.5$, $v_b = 0.014$, and $a_b = 0.51$), and the accretion rates in units of \dot{M}_{Edd} are exactly same. Although the radiative moments around a super-massive BH are significantly different, yet the v profiles differ by moderate amount. To ascertain the cause we plot \mathfrak{R} or relative contribution of radiative moments for both the jets in Fig. 10b. \mathfrak{R} is quite similar for both the BHs close to the horizon, but in the range $4 < z < 10$ \mathfrak{R} around stellar mass BH is higher than that around super massive BH. In Fig. 10c, we compare the Lorentz factor γ of a jet around

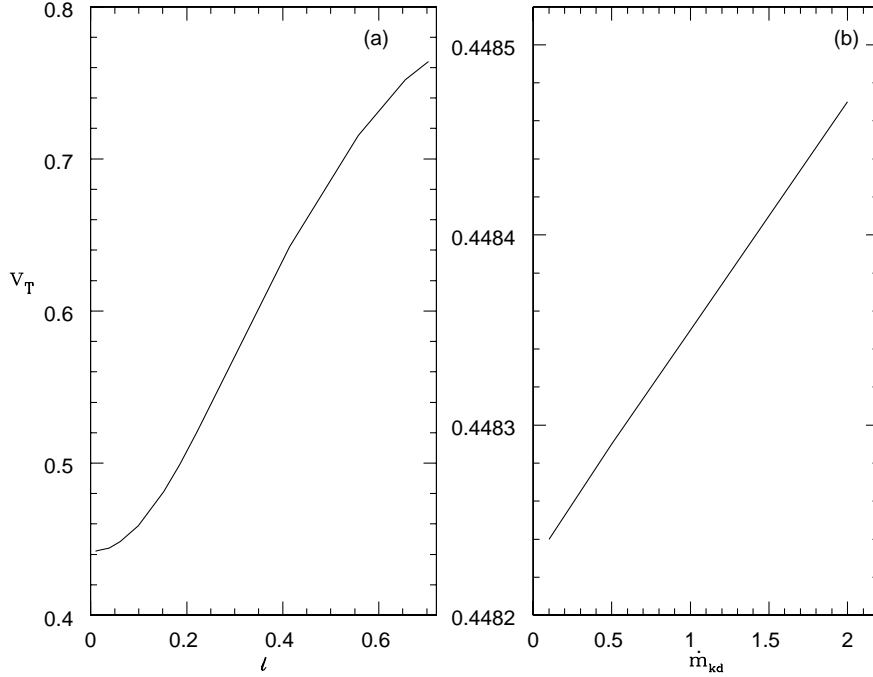


Figure 9. Dependence of terminal speeds v_T on (a) l and on (b) \dot{m}_{kd} for the same base values of jet ($z_b = 1.5$, $v_b = 0.014$, $a_b = 0.51$). The value of $\dot{m}_{kd} = 1$ for (a), and $\dot{m}_{sk} = 5$ for (b). While $\beta = 0.5$ for both the cases.

$10M_\odot$ BH (solid, black online) with a jet 10^8M_\odot (dotted, blue online), launched with hot base ($z_b = 1.5$, $v_b = 0.19$, $a_b = 0.576$) and acted by high accretion rate $\dot{m}_{sk} = 12$. The initial jet γ ($\equiv v$) is almost same for both the jets, however, due to larger \mathfrak{R} around a stellar mass BH, the jet around it slower compared to that around super-massive BH. In this case, the terminal Lorentz factor γ_T is significantly larger for a jet around 10^8M_\odot BH.

It is clear that jets around stellar mass BH are slower, and lighter jets are faster, but what is the maximum terminal velocity possible? We choose to launch jet with maximum possible sound speed at the base and very high accretion rate. In Fig. 11, we plot the maximum terminal Lorentz factor or $\gamma_{T\max}$ possible as a function of ξ for $10M_\odot$ BH (solid, black online) and 10^8M_\odot (dotted, blue online), when accretion parameters are $\dot{m}_{sk} = 12$, $\beta = 0.5$ and $\dot{m}_{kd} = 1$. For jet composition $\xi = 1.0$, the maximum possible terminal Lorentz factor $\gamma_{T\max} \lesssim 9$ for a jet around $10M_\odot$ BH, but for 10^8M_\odot BH, $\gamma_{T\max} \gtrsim 11$. However, for lighter jet around stellar mass BH $\gamma_{T\max} \sim 10$, but for super-massive BH, light jets yields

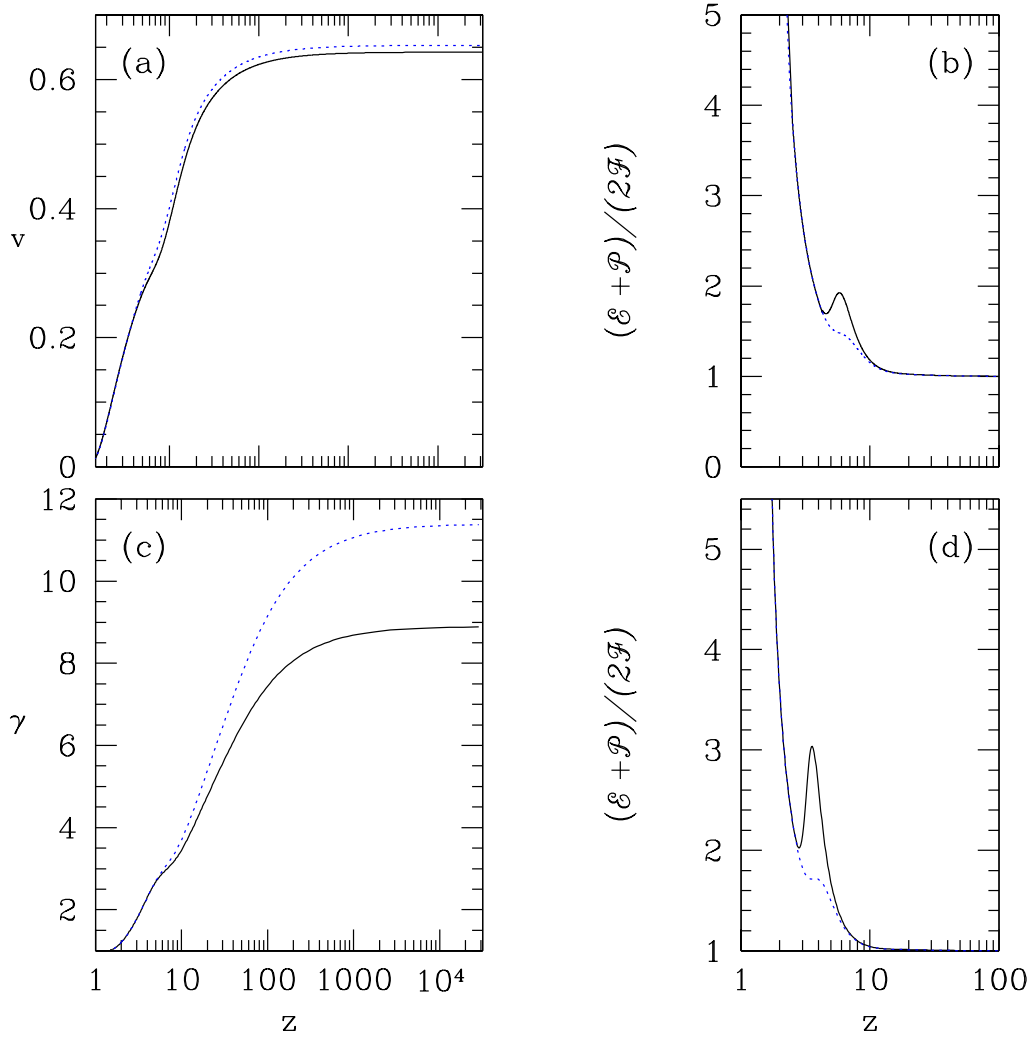


Figure 10. Comparison of (a) v profile for jets around $10M_{\odot}$ (solid, black online) and 10^8M_{\odot} black holes (dotted, blue online). The SKD accretion rate is $\dot{m}_{\text{sk}} = 10$. (b) $\mathfrak{R} = (\mathcal{E} + \mathcal{P})/2\mathcal{F}$ with z from an accretion disc around $10M_{\odot}$ BH (solid, black online) and 10^8M_{\odot} BH (dotted, blue online). The jet base values for (a) and (b) are $z_b = 1.5$, $v_b = 0.014$, and $a_b = 0.51$. (c) γ profile of a jet around $10M_{\odot}$ BH (solid, black online) and 10^8M_{\odot} (dotted, blue online). (d) $\mathfrak{R} = (\mathcal{E} + \mathcal{P})/2\mathcal{F}$ with z . The SKD parameter is $\dot{m}_{\text{sk}} = 12$. Other disc parameters are $\dot{m}_{\text{kd}} = 1$, $\beta = 0.5$. And the jet base values for (c) and (d) are $z_b = 1.5$, $v_b = 0.19$, and $a_b = 0.576$.

$\gamma_{T\text{max}} \sim \text{few} \times 10$. So for light jets ultra-relativistic jets around super-massive BH is possible if it is driven by the radiation from a luminous disc.

5 DISCUSSION AND CONCLUDING REMARKS

In this paper, we have investigated the interaction of a relativistic fluid-jet with the radiation field of the underlying accretion disc. The accretion disc plays an auxiliary role, in other words, the jet-disc connection has been ignored in the present study. In principle the accretion rates, and the outer boundary condition, determines the jet states, as well as, the radiation field around it. We reduced the number of free parameters to determine the

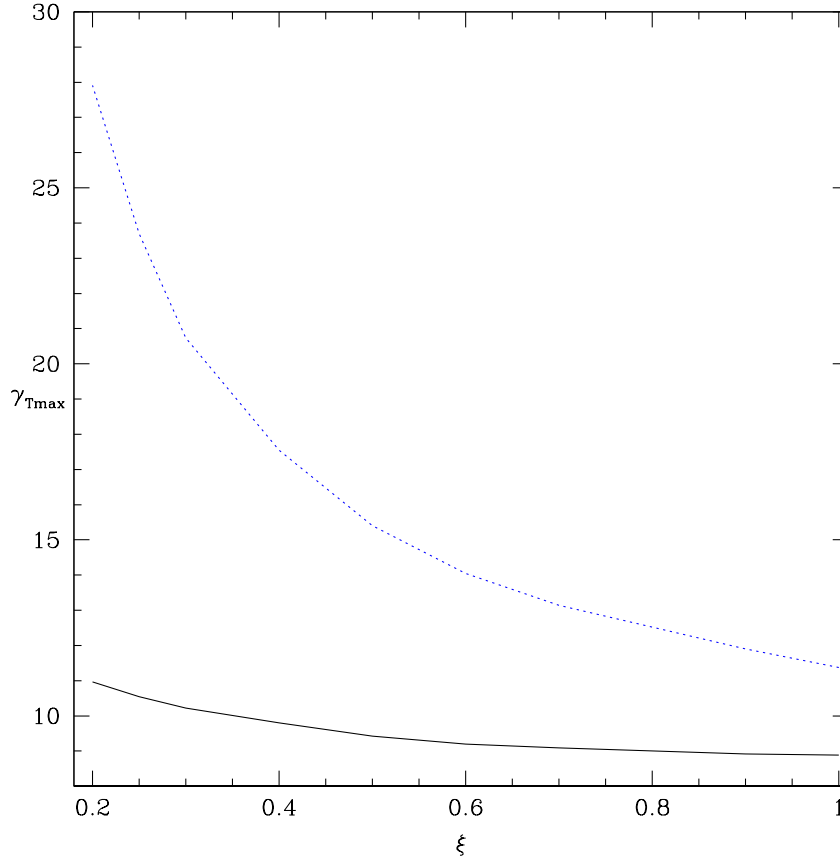


Figure 11. Variation of $\gamma_{T\max}$ with ξ , around $10M_{\odot}$ BH (solid, black online) and 10^8M_{\odot} BH (dotted, blue online). Accretion parameters are $\dot{m}_{\text{sk}} = 12$, $\beta = 0.5$ and $\dot{m}_{\text{kd}} = 1$. and jet base values are $z_b = 1.5$, & $a_b = 0.5766$.

radiation field, by estimating the temperature, density and the velocity profile of the various components of the accretion disc and considered them as generic (Appendix A). The radiative intensities of the SKD is determined from the estimated temperature, density and the velocity profile by supplying the accretion rates of \dot{m}_{sk} (Appendix A). The same for KD is obtained only from the \dot{m}_{kd} . We used some known accretion disc solutions from the literature (Kumar & Chattopadhyay 2014), to obtain a simplifying analytic relation between the shock location and the SKD accretion rate (Appendix B). This enables us to reduce one free parameter (*i.e.*, x_s). Now we use those same accretion disc solutions in the general radiative transfer code (Mandal & Chakrabarti 2008), and compute the spectra, as well as, ratio of the luminosities from the PSD and the pre-shock disc as a function of shock location (Appendix B). In other words, the accretion rates determine the accretion solutions and the shock location, which determines the disc luminosities, intensities and therefore the entire radiation field around it. And then we studied the propagation of a transonic and relativistic jet through this radiation field.

We noticed that proper relativistic transformation of the radiative intensities from the local disc frame to the observer frame is very important and these transformations modify the magnitude, as well as, the distribution of the moments around a compact object. The PSD and SKD are the major contributors in the net radiative moments and KD contribution is much lower than either one of the former two. However, the contribution of PSD compared to that of SKD in the net moment, will depend on where the shock forms which is also dictated by the accretion rate. One of the interesting fact about the moments due to various disc components is that they peak at different positions away from the disc plane. Therefore the jet which is initially thermally driven, but is further accelerated by the radiative moments from various disc components further down stream. The jets with normal conditions at the base, produces mildly relativistic jets with terminal velocities $v_T \sim \text{few} \times 0.1$ (Fig. 6). The scattering regime maintains the isentropic nature of the jet, and because we considered a realistic and relativistic gas equation of state, the adiabatic index changes along the jet. However, radiation not only accelerates but also decelerates if $v > v_{\text{eq}}$. Although close to the jet base (z_b) the velocity is low and the radiation field should accelerate, but being hot the effect of radiation is not significant in the subsonic branch because of the presence of inverse of enthalpy term in the radiative term a_r of the equation of motion (equation 15). Therefore, in the subsonic domain the jet is accelerated as a result of competition between thermal and the gravity term. In the supersonic domain the gravity term is smaller than both the thermal and the radiative term. If $a_r < 0$ and $|a_r| \gtrsim a_t$, then the jet can be decelerated (Figs. 7a,b). As the magnetic pressure is increased, the synchrotron radiation from SKD increases and it jacks up the flow velocity in the supersonic regime. Increasing the \dot{m}_{sk} increases both the synchrotron, as well as, bremsstrahlung photons from the SKD, which makes the SKD contribution to the net radiative moment more dominant, and therefore increases the v in the supersonic part of the flow. The v_T increases with β but tends to taper off as $\beta \rightarrow 1$, however, v_T tends to increase with \dot{m}_{sk} and shows no tendency to taper off. The jet tends to get faster with the decrease in protons (*i.e.*, decrease of ξ). We do not extend our study to electron and positron or $\xi = 0$ jet, since a purely electron-positron jet is highly unlikely (Kumar *et al.* 2013), although pair dominated jet (*i.e.*, $0 < \xi < 1$) is definitely possible. So we extend our study to $0.27 \leq \xi \leq 1$ jets (Fig. 8a-f). Although the terminal velocity v_T increases with the total luminosity ℓ , and approaches relativistic values as the disc luminosity approaches the Eddington limit. However, the KD plays a limited role in accelerating jets (Figs. 9 a,b). Since the radiation field around a super-massive BH and stellar mass BH is

different, we compared jets starting with the same base values, same accretion rates (in units of \dot{M}_{Edd}) but around stellar mass and super-massive BH. If accretion rates are moderately high, then jets around super-massive BHs are slightly faster than those around stellar mass BH (Figs. 10a, b). However, if accretion rates are high such that the moments from the central region of the disc differ significantly, then ultra-relativistic jets around super massive BHs can be obtained compared to stellar mass BH (Figs. 10c, d). For high accretion rates, it has been shown that around stellar mass BH, moments due to PSD and the pre-shock disc are comparable, which makes $\mathfrak{R} > 1$ for a larger distance away from the BH (Fig. 4). This limits the maximum velocity a jet may achieve around a stellar mass BH, compared to that around a super-massive BH. This brings us to the issue of maximum possible terminal velocity of the jet. We launched jets with relativistic sound speed in order to get maximum thermal driving, while increase the accretion rates to very high values. The comparison of jet $\gamma_{T\text{max}}$ around a stellar mass BH and that around super massive one as a function of ξ , shows that jet around super massive BH can be accelerated to $\gamma_T \gtrsim 11$ even for fluid composition $e^- - p^+$, while that around stellar mass BH $\gamma_T \sim \text{few}$. However, lighter jets around $10^8 M_\odot$ BH can be accelerated to truly ultra-relativistic speeds, compared to jets around stellar mass BH.

It is interesting that the radiative moments from different disc components maximize at different distances from the jet base, which opens up the possibility of multi stage acceleration of the jet. However, close to the base, thermal acceleration is the main driving force that makes the flow supersonic, and thereby negating the effect of gravity. Thereafter, the radiative driving accelerates jet to mildly relativistic terminal velocities if the radiation field is mild, but intense radiation field can accelerate jets to ultra-relativistic velocities. Hence, the thermal driving of the jet at the base, along with the radiative driving further out, comprises a complete multi-stage acceleration rather than just the radiation field itself. Although the maximum terminal speeds achieved is truly ultra-relativistic, especially around super-massive BHs, but at the jet base, which is hot, the disc photons may take away energy from the hot electrons instead of imparting its momentum onto it. The jet base may also radiate via other processes. These radiations would, in the observer frame, actually be flowing along the jet and therefore may interact and deposit momentum on to the jet further down stream. The jet may also gain energy via free-free absorption. These aspects have been ignored and therefore the conclusions might slightly differ. However, it is clear the jet can be accelerated to relativistic terminal speed. We would like to simulate the present

work of radiation driven relativistic jets around compact objects, similar to our effort with galactic outflows (Chattopadhyay *et al.* 2012). One of the major difference expected is, if the radiative states of the accretion disc changes, how does it affect the jet and what are the timescales in which these changes are expected to be observed in the jets. These advances of our work are underway and will be reported elsewhere.

ACKNOWLEDGMENT

The authors acknowledge the anonymous referee for helpful suggestions.

REFERENCES

- Biretta J. A., 1993, in Burgerella D., Livio M., Oea C., eds, Space Telesc. Sci. Symp. Ser., Vol. 6, Astrophysical Jets. Cambridge Univ. Press, Cambridge, p. 263
- Chakrabarti S.K., ApJ, 1989, 347, 365
- Chakrabarti, S K., Titarchuk, L., 1995, ApJ, 455, 623.
- Chandrasekhar, S., 1938, An Introduction to the Study of Stellar Structure, Dover, NewYork.
- Chattopadhyay, I., Chakrabarti, S. K., 2000a, Int. Journ. Mod. Phys. D, 9, 57.
- Chattopadhyay, I., Chakrabarti, S. K., 2000b, Int. Journ. Mod. Phys. D, 9, 717.
- Chattopadhyay, I., Chakrabarti, S. K., 2002, MNRAS, 333, 454.
- Chattopadhyay, I., Das, S., Chakrabarti, S. K., 2004, MNRAS, 348, 846.
- Chattopadhyay I., 2005, MNRAS, 356, 145.
- Chattopadhyay, I.; Das, S., 2007, New A, 12, 454.
- Chattopadhyay, I., 2008, in Chakrabarti S. K., Majumdar A. S., eds, AIP Conf. Ser. Vol. 1053, Proc. 2nd Kolkata Conf. on Observational Evidence of Black Holes in the Universe and the Satellite Meeting on Black Holes Neutron Stars and Gamma-Ray Bursts. Am. Inst. Phys., New York, p. 353
- Chattopadhyay I., Ryu D., 2009, ApJ, 694, 492
- Chattopadhyay I., Chakrabarti S.K., 2011, Int. Journ. Mod. Phys. D, 20, 1597.
- Chattopadhyay, I., Sharma, M., Nath, B. B., Ryu, D., 2012, MNRAS, 423, 2153.
- Chattopadhyay I., Ryu D., Jang, H., 2013, ASInc, 9, 13.
- Cox J. P., Giuli, R. T., 1968, Principles of stellar structure, Vol. 2, Gordon and Breach Science Publishers, New York.

- Das, S., Chattopadhyay, I., Nandi, A., Molteni, D., 2014, 442, 251.
- Doeleman S. S. et al., 2012, *Science*, 338, 355.
- Fender, R. P., Gallo, E., Russell, D., 2010, *MNRAS*, 406, 1425.
- Ferrari, A., Trussoni, E., Rosner, R., Tsinganos, K., 1985, *ApJ*, 294, 397.
- Fukue, J., 1987, *PASJ*, 39, 309
- Fukue, J., 1996, *PASJ*, 48, 631
- Fukue, J., 1999, *PASJ*, 51, 425
- Fukue, J., Tojyo, M., Hirai, Y., 2001, *PASJ* 53 555
- Gallo, E., Fender, R. P., Pooley, G., G., 2003 *MNRAS*, 344, 60
- Giri, K., Chakrabarti, S. K., 2013, *MNRAS*, 430, 2826
- Hirai, Y, Fukue, J., 2001, *PASJ*, 53, 285
- Hsieh, H. S., Spiegel, E. A., 1976, *ApJ*, 207, 244
- Icke, V., *AJ*, 85, 329.
- Icke, V., *A&A*, 216, 294.
- Junor W., Biretta J.A., Livio M., 1999, *Nature*, 401, 891
- Kato, S., Fukue, J., Mineshige, S., 1998, *Black-hole Accretion Disks*. Kyoto Univ. Press, Kyoto.
- Kumar R., Chattopadhyay I., 2013, *MNRAS*, 430, 386.
- Kumar R., Singh, C. B., Chattopadhyay, I., Chakrabarti, S. K., 2013, *MNRAS*, 436, 2864.
- Kumar R., Chattopadhyay I., Mandal, S., 2014, *MNRAS*, 437, 2992.
- Kumar R., Chattopadhyay I., 2014, *MNRAS*, 443, 3444.
- Liang, E. P. T., Thompson, K. A., 1980, *ApJ*, 240, 271L
- Mandal, S., Chakrabarti, S. K., 2008, *ApJ*, 689, 17L.
- Melia, F., Königl, A., 1989, *ApJ*, 340, 162
- Mihalas, D., Mihalas, B. W., 1984, *Foundations of Radiation Hydrodynamics*. Oxford University Press, Oxford.
- Molteni, D., Lanzafame, G., Chakrabarti, S. K., 1994, *ApJ*, 425, 161
- Molteni, D., Ryu, D., Chakrabarti, S. K., 1996, *ApJ*, 470, 460
- Mirabel I. F., Rodriguez L. F., 1994, *Nat*, 371, 46
- Narayan, R., Kato, S., Honma, F., 1997, *ApJ*, 476, 49
- Paczynski, B. and Wiita, P.J., 1980, *A&A*, 88, 23
- Rushton, A., Spencer R., Fender, R., Pooley, G., 2010, *A&A*, 524, 29.
- Ryu, D., Chattopadhyay, I., Choi, E., 2006, *ApJS*, 166, 410.

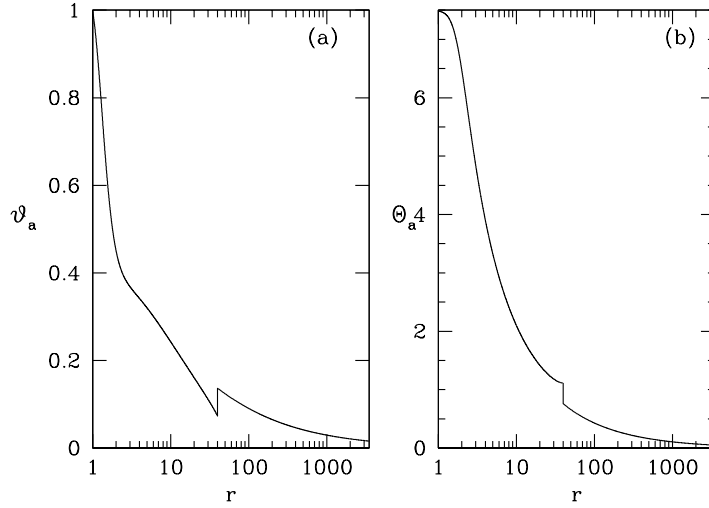


Figure A1. Velocity v_a and dimensionless temperature Θ_a estimated for accreting flow for angular momentum $\lambda = 1.7$. Here $r_0 = 3500$ and $v_0 = 0.01$.

Shapiro, S. L., Teukolsky, S. A., 1983, *Black Holes, White Dwarfs and Neutron Stars, Physics of Compact Objects*. Wiley-Interscience, New York.

Sikora, M., Wilson, D. B., 1981, *MNRAS*, 197, 529.

Sikora, M., Sol, H., Begelman, M. C., Madejiski, G. M., 1996, *MNRAS*, 280, 781.

Shakura, N. I., Sunyaev, R. A., 1973, *A&A*, 24, 337S.

Svensson, R.; 1982, *ApJ*, 258, 335

Synge, J. L., 1957, *The Relativistic Gas*, Amsterdam, North Holland.

Taub A.H., 1948, *Phys. Rev.*, 74,

Zensus J. A., Cohen M. H., Unwin S. C., 1995, *ApJ*, 443, 35

APPENDIX A: ESTIMATION OF TEMPERATURE AND VELOCITY OF SKD AND PSD

In the present analysis, the focus rests upon outflows and the accretion disc plays an auxiliary role, as radiation from the various accretion disc components affect the jet dynamics. Since the accretion disc emission depends on the flow variables of the disc, we need to know the temperature and velocity distribution. The method to estimate the velocity distribution of

SKD and PSD are given below. We estimate the velocity from geodesic equations, which shows that the covariant time component of four velocity *i.e.*, u_t is a constant of motion. From $u_\mu u^\mu = -1$, find Now,

$$-u_t u^t = -g^{tt}(u_t)^2 = \gamma^2 = \gamma_\vartheta^2 \gamma_\phi^2 \equiv \text{square of Lorentz factor},$$

where,

$$\gamma_{\vartheta_a}^2 = \frac{1}{1 - \vartheta_a^2}; \quad \gamma_\phi^2 = \frac{1}{1 - v_{\phi a}^2}; \quad v_{\phi a}^2 = \frac{-u_\phi u^\phi}{u_t u^t} = \frac{(r-1)\lambda^2}{r^3}. \quad (\text{A1})$$

Here, ϑ_a is the radial 3-velocity measured by a co-rotating observer, while the radial 3-velocity is v_{ra} , and are defined as

$$v_{ra}^2 = \frac{-u_r u^r}{u_t u^t}; \quad \& \quad \vartheta_a^2 = \gamma_\phi^2 v_{ra}^2$$

The suffix ‘a’ stands for either PSD, SKD or KD. For KD $v_{rkd} = \vartheta_{kd} = 0$ and $v_{\phi kd}$ is the Keplerian azimuthal velocity. We chose outer boundary conditions ($\vartheta_a = \vartheta_{0a}$, and λ_0 at $r = r_0$), this relation allows us to calculate u_t for SKD,

$$(u_t)^2|_{r_0} = \left(1 - \frac{1}{r_0}\right) \frac{1}{1 - \vartheta_{0a}^2} \cdot \frac{r_0^3}{r_0^3 - (r_0 - 1)\lambda_0^2}. \quad (\text{A2})$$

And then from equation A2 we obtain $\vartheta(r)_{sk}$,

$$\vartheta_{sk} = \left[1 - \frac{(r-1)r^2}{\{r^3 - [(r-1)\lambda^2]\}u_t^2|_{r_0}}\right]^{1/2}. \quad (\text{A3})$$

Here, the equations are expressed in geometric units $2G = M_B = c = 1$. One must note from equation (A3) that as $r \rightarrow 1$, $\vartheta \rightarrow 1$, although SKD in presence of shock, does not extend upto the horizon. However, one should also remember since the velocity is obtained from geodesic equations, it is slightly over estimated because the pressure gradient terms were ignored while estimating the velocity. This would under estimate the radiative moments slightly and hence our results are believable since there is no over estimation of jet and radiation interaction. To get the velocity distribution for the PSD, we assume the shock compression ratio is 3, so the ratio of post shock (suffix +) and preshock (with suffix -) velocities are $\vartheta_+ = \vartheta_-/3$ at $r = x_s$, with this boundary condition we recalculate the constant of motion and then use it to estimate the ϑ distribution for PSD,

$$\vartheta_{ps} = \left[1 - \frac{(r-1)r^2}{\{r^3 - [(r-1)\lambda^2]\}u_t^2|_{x_s}}\right]^{1/2}. \quad (\text{A4})$$

In Fig. (A1a) we have plotted the velocity distribution of SKD and PSD, where the suffix ‘a’ signifies either sk or ps.

A1 Density and temperature of SKD

The SKD accretion rate equation is

$$\dot{M}_{\text{sk}} \approx \rho_{\text{sk}} u_{\text{sk}}^r r H_{\text{sk}}, \quad (\text{A5})$$

here H_{sk} is the local height of SKD. If the outer boundary of the accretion disc is at r_0 , the height at outer boundary H_0 , the radial four velocity u_0^r , the dimensionless temperature Θ_0 and the density ρ_0 , then we have

$$\frac{\rho_{\text{sk}}}{\rho_0} = \frac{u_0^r r_0 H_0}{u_{\text{sk}}^r r H_{\text{sk}}} \quad (\text{A6})$$

Here, u_{sk}^r is obtained from equation A3 and $H_{\text{sk}} = r \cot \theta_{\text{sk}} + d_0$.

Assuming fixed Γ and moderate radiative loss, then the dimensionless temperature or $\Theta_{\text{sk}} = p_{\text{sk}}/\rho_{\text{sk}}c^2$ is given by,

$$\Theta_{\text{sk}} = \Theta_0 \left(\frac{\rho_{\text{sk}}}{\rho_0} \right)^{\Gamma-1} = \Theta_0 \left(\frac{u_0^r r_0 H_0}{u_{\text{sk}}^r r H} \right)^{\Gamma-1} \quad (\text{A7})$$

Equations (A7 and A6) are used to compute the intrinsic synchrotron and bremsstrahlung intensity of the SKD. Using the expression of $u_a^r = (1 - 1/r)^{1/2} \gamma_{\vartheta_a} \vartheta_a$, in equation A7, the SKD and PSD temperature distribution can be obtained. In Fig. (A1b), the dimensionless temperature distribution Θ_a is plotted for both SKD and PSD.

APPENDIX B: RELATION BETWEEN \dot{M}_{sk} AND X_S

In Fig. (B1a) red triangles represent the locations of shock for a given \dot{m}_{sk} . Other parameters are $r_0 = 3686$, $\vartheta_0 = 1.928 \times 10^{-3}$, $\Theta_0 = 9.811 \times 10^{-2}$, $\lambda_0 = 1.7$ and the viscosity parameter $\alpha = 0.001$. In the figure, x_s is computed using the methods of Kumar & Chattopadhyay (2014) for the given values of α , \dot{m}_{sk} , r_0 , ϑ_0 , Θ_0 and λ_0 . We fitted a curve using these data generated by Kumar & Chattopadhyay (2014) and expressed x_s as a function \dot{m}_{sk} , the explicit form of which is

$$x_s = 64.8735 - 14.1476 \dot{m}_{\text{sk}} + 1.24286 \dot{m}_{\text{sk}}^2 - 0.039467 \dot{m}_{\text{sk}}^3. \quad (\text{B1})$$

Therefore, while calculating the radiative moments, x_s is no more a free parameter, but is estimated using equation (B1).

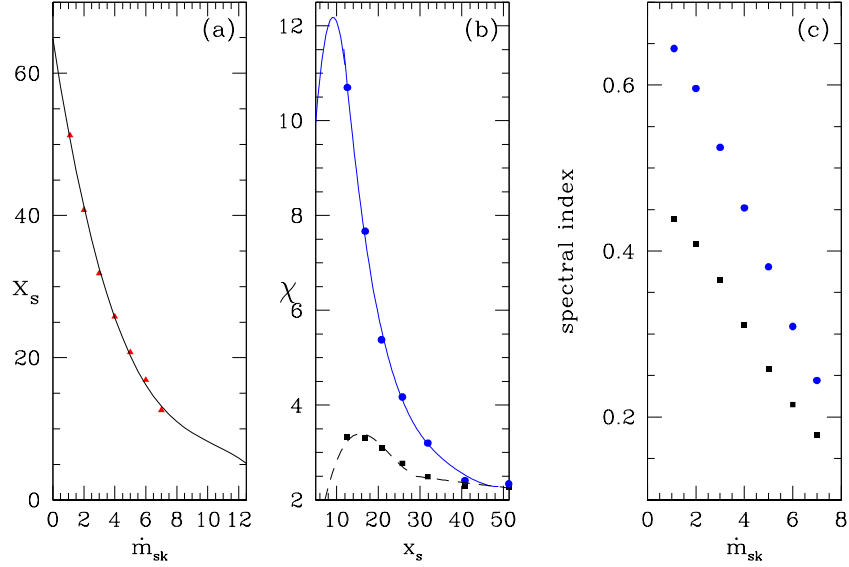


Figure B1. (a) Shock location x_s as a function of \dot{m}_{sk} (filled triangles, red online). The fitted function given by equation (B1) (solid curve, black online). Parameters fixed to get the data (filled triangles) are $r_0 = 3686$, $\vartheta_0 = 1.928 \times 10^{-3}$, $\Theta_0 = 9.811 \times 10^{-2}$, $\lambda_0 = 1.7$ and $\alpha = 0.001$. (b) χ as a function of x_s for $10M_\odot$ (filled square, black online) and 10^8M_\odot BH (filled circle, blue online). The corresponding fitted functions for $10M_\odot$ BH (dashed, black online) and 10^8M_\odot BH (solid, blue online) presented in equations (B3, B4). (c) Spectral index as a function of \dot{m}_{sk} plotted for the same data points of Fig. a. for $10M_\odot$ BH (filled square, black online) and 10^8M_\odot BH (filled circle, blue online).

B1 Obtaining relation between shock location and ratio of pre-shock and post-shock luminosities

In previous works in which radiatively driven jets were studied (Chattopadhyay & Chakrabarti 2000b, 2002; Chattopadhyay *et al.* 2004; Chattopadhyay 2005), the luminosity from PSD (ℓ_{ps}) was supplied as a free parameter, but in the present work, we calculate this from spectral modeling. KD produces the well known thermal radiation (Shakura & Sunyaev 1973), while SKD emits via bremsstrahlung and synchrotron emission. For the same set of outer boundary conditions, *i.e.*, α , \dot{m}_{sk} , r_0 , ϑ_0 , Θ_0 and λ_0 and \dot{m}_{kd} at r_0 , we solve the general radiative transfer equations similar to those by Chakrabarti & Titarchuk (1995); Mandal & Chakrabarti (2008). For the disc parameters of Fig. B1a, the shock location varied between $51.25 \geq x_s \geq 12.6$ as one varied $1.1 \leq \dot{m}_{sk} \leq 7$, keeping all other boundary conditions same. The flow solutions of Kumar & Chattopadhyay (2014) were obtained in a

unit system where $M_B = 1$, so the actual luminosity and spectra will depend on the mass of the central object. PSD being optically slim will inverse-Comptonize radiations coming from pre-shock disc (SKD and KD). Let the luminosity from SKD and KD be denoted as ℓ_{ps} and ℓ_{kd} . Then the ratio of luminosities is defined as $\chi = \ell_{\text{ps}}/(\ell_{\text{sk}} + \ell_{\text{kd}})$. In Fig. (B1b) we plot χ with x_s for the same set of data points as in Fig. (B1a) and considering $\dot{m}_{\text{kd}} = 1$, we obtain the spectra and luminosities of each disc component for $M_B = 10M_\odot$ (black, squares) and $M_B = 10^8M_\odot$ (blue, circles).

The behaviour of χ for 10^8M_\odot is different from that of $10M_\odot$ because synchrotron cooling is very efficient for a stellar mass black hole. For a $10M_\odot$ black hole, the post-shock luminosity increases initially as the post-shock flow is still very hot but as shock location moves close to black hole, \dot{m}_{sk} is very high and pre-shock synchrotron cooling becomes large enough to reduce the ratio (χ). On the other hand χ keeps on increasing for 10^8M_\odot because Comptonization due to Keplerian soft photons is the most efficient cooling process and as shock moves in, the supply of hot electron increases (as \dot{m}_{sk} increases) which enhances the post-shock luminosity. In Fig. (B1c) we plot the variation of spectral index with \dot{m}_{sk} . We see that as \dot{m}_{sk} increases the spectral states becomes harder because supply of hot the electron increases. Moreover, the spectral index for a super-massive black hole is generally softer than a stellar mass black hole as the PSD of stellar mass black hole is relatively hotter. We fitted the plots of Fig. (B1b) with analytic functions (the constants are written correct up to three decimal points) given by

$$\chi_8 = 25.944 - 1.667x_s + 3.992 \times 10^{-2}x_s^2 - 3.199 \times 10^{-4}x_s^3 \quad (x_s > 12); \quad (\text{B2})$$

$$\chi_8 = 1.449 + 2.336x_s - 0.127x_s^2. \quad (x_s \leq 12)$$

$$\chi_1 = -2.525 + 0.913x_s - 4.438 \times 10^{-2}x_s^2 + 6.522 \times 10^{-4}x_s^3 \quad (x_s \leq 29); \quad (\text{B3})$$

$$\chi_1 = -2.914 - 1.622 \times 10^{-2}x_s + 7.265 \times 10^{-5}x_s^2 + 1.278 \times 10^{-7}x_s^3 \quad (x_s > 29).$$

Here, χ_8 signifies the ratio of PSD to SKD+KD luminosity for $M_B = 10^8M_\odot$ (blue, solid curve Fig. B1b), while χ_1 is the ratio of luminosities for $M_B = 10M_\odot$ (black, dashed curve Fig. B1b). Therefore we supply \dot{m}_{sk} and parameters at the outer boundary and estimate the ϑ_{sk} , Θ_{sk} and ρ_{sk} . up to the x_s (obtained via equation B1) and these solutions we obtain ℓ_{sk} . The ℓ_{kd} can be estimated from \dot{m}_{kd} , r_0 (outer edge) and x_s (inner edge). So from the preshock luminosity ($\ell_{\text{sk}} + \ell_{\text{kd}}$) we can estimate the ℓ_{ps} using either expression (B4) or (B3)

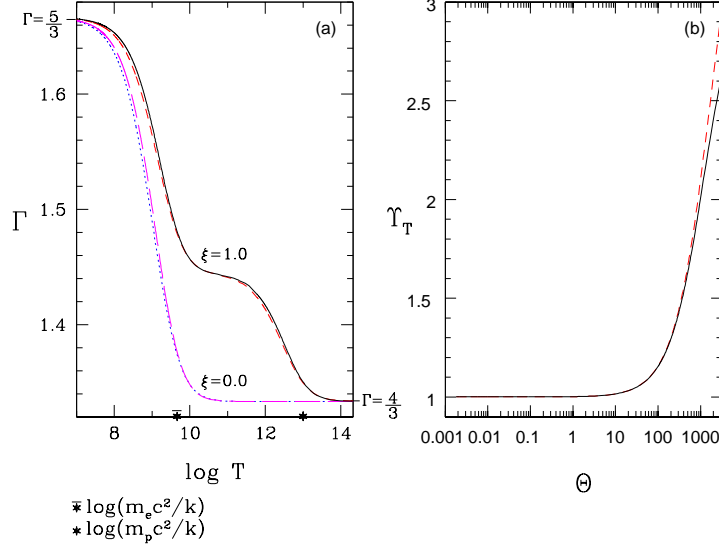


Figure C1. (a) Comparing adiabatic index Γ as a function of temperature T , for RP EoS (solid, black online and long dashed, magenta online). CR EoS is presented by dashed curve (red online) and dotted (blue online) curves. The two separate cases $\xi = 0$ and $\xi = 1$ are marked on the curves. Temperature corresponding to electron and proton rest mass are also marked on the T axis. (b) Υ_T as a function of Θ for $e^- - p^+$ flow, but for RP EoS (solid, black online) and CR EoS (dashed, red online).

depending on the central mass. In this work $10M_\odot$ is considered as a representative of stellar mass BH and 10^8M_\odot is considered as super massive BH.

APPENDIX C: EQUATION OF STATE

The EoS for relativistic fluid is obtained by integrating the relativistic energy of fluid particles following a relativistic Maxwell-Boltzman distribution in the momentum space as was obtained by Chandrasekhar (1938); Synge (1957); Cox & Giuli (1968). For single species fluid the different forms of the EoS obtained by the above authors are as below,

$$e_C = \rho c^2 \frac{3K_3(1/\Theta) + K_1(1/\Theta)}{4K_2(1/\Theta)}; \quad e_S = \rho c^2 \frac{K_3(1/\Theta)}{K_2(1/\Theta)} - p; \quad e_{CG} = \rho c^2 \left(3\Theta + \frac{K_1(1/\Theta)}{K_2(1/\Theta)} \right), \quad (C1)$$

where, e represents local energy density of the flow, Θ the measure of temperature and suffix C, S, and CJ signifies Chandrasekhar, Synge and Cox & Giuli, respectively. The K 's are modified Bessel's functions of second kind and respective indices indicate their degree.

We recall the recurrence relation $K_{m+1}(x) = K_{m-1}(x) + 2mK_m/x$, and obtain

$$h_C = \frac{e + p}{\rho c^2} = \frac{3K_3}{4K_2} + \frac{K_1}{4K_2} + \Theta = \frac{K_1}{K_2} + 4\Theta = h_S = h_{CG} \quad (C2)$$

Therefore, all the forms of exact EoS for relativistic gas presented above, are equivalent, and let us denote the EoS represented by equation (C1) as 'relativistically perfect' or RP EoS.

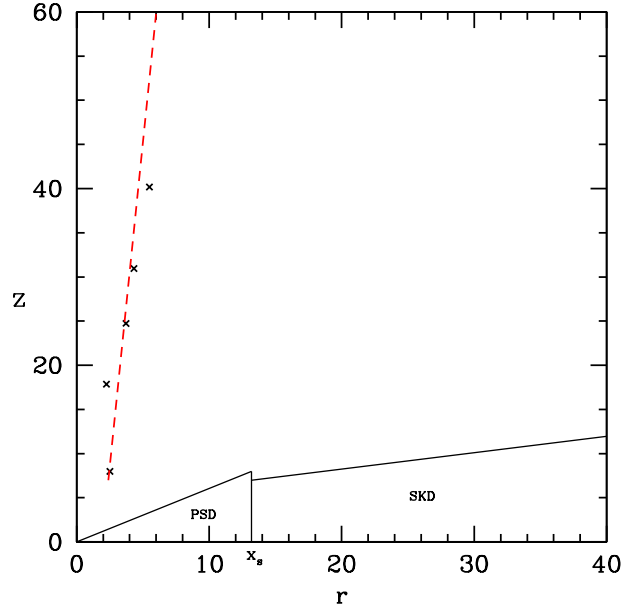


Figure D1. Estimated width of the jet by (crosses) by matching the thermal, gravity and radiative forces along r , for jet base values $z_b = 1.5$, $a_b = 0.50544$, $v_b = 0.00345$ and disk parameters $\dot{m}_{\text{sk}} = 7$ and $\dot{m}_{\text{kd}} = 1$. The conical cross-section approximation is shown by a fitted line (dashed, red online). The disc top surface and disc components (PSD and SKD) shown, is estimated from accretion rates supplied.

The multispecies approximate EoS used in this paper, may be called Chattopadhyay-Ryu or CR EoS (equation 10), not only mimics equation (C1) very well, but also satisfies the fundamental inequality obtained by Taub (1948). Taub showed from first principle that any EoS for dilute relativistic gas have to satisfy a fundamental in-equality given by

$$\Upsilon_T = \left(h - \frac{p}{\rho c^2} \right) \left(h - \frac{4p}{\rho c^2} \right) \geq 1. \quad (\text{C3})$$

By following equation (12), we can calculate Γ for any EoS. In Fig. (C1a) we plot adiabatic index Γ as a function of temperature T , for $e^- - p^+$ (marked $\xi = 1$) and $e^- - e^+$ (marked $\xi = 0$) flow. For $e^- - p^+$ flow, the solid curve (black online) is the Γ with RP EoS, and dashed curve (red online) is the Γ with CR EoS. And for $e^- - e^+$ flow, Γ with RP EoS is the long dashed (magenta online) curve, and that due to CR is dotted (red online) curve. In Fig. (C1b) we compare the Taub function Υ_T as a function of Θ for $e^- - p^+$ flow described by RP EoS (solid, black online) and CR EoS (dashed, blue online). Both the EoS comfortably satisfy the in-equality.

APPENDIX D: ON THE JET GEOMETRY

In this paper we assumed the flow surface of the jet to be conical having a small opening angle and maintains it throughout the spatial extent. Here we test how good is the approximation. To approximately locate the lateral extent of the jet, we balance the pressure gradient term, the gravity term and the radiative term along r direction. We assume that $\partial p/(\rho \partial r)$ at the jet edge is equal to $\partial p/(\rho \partial z)$ on the axis. So

$$a_{p_r} = -\frac{1}{\rho} \frac{\partial P}{\partial r} \approx \frac{2\Gamma\Theta}{\tau} \left(\frac{\gamma^2}{v} \frac{dv}{dz} + \frac{2}{z} \right) \quad (\text{D1})$$

Similarly, approximating $u^r \approx u^\phi \approx 0$, the component of the radiative term along r can be evaluated as (see, equation 3a of Chattopadhyay 2005),

$$a_{r_r} = \gamma (\mathcal{F}^r - v\mathcal{P}^{rz}) \quad (\text{D2})$$

The gravity term is

$$a_{g_r} = \frac{r}{2R(R-1)^2}; \quad R = (r^2 + z^2)^{1/2} \quad (\text{D3})$$

In Fig. (D1) we plot the location where $|a_{p_r}| = |a_{r_r} + a_{g_r}|$ for a radiation field due to disc parameters $\dot{m}_{sk} = 7$, $\dot{m}_{kd} = 1$ and jet characterized by $z_b = 1.5$, $a_b = 0.50544$, $v_b = 0.00345$. The accretion disc upper surface is also shown in the figure. The locations where $|a_{p_r}| = |a_{r_r} + a_{g_r}|$, is shown by crosses. The approximated boundary of the jet (dashed, red online), shows consideration of conical jet flow geometry is a fairly good assumption. Although, this assumption is reasonable only when the jet opening angle is small. This is because for large opening angle, jet material at the edges would be spun up by \mathcal{F}^ϕ , which may contribute in spreading the jet.